reaction was performed according to the protocol of the manufacturer using 20 μg of protein collected from the sample. The protein sample was incubated with a blot array precoated with 40 cytokine/chemokine antibodies overnight at 4 °C. These blots were visualized using Lumi GLO Reserve Chemiluminescent Substrate Kit (Cell Signaling Technology) and quantified by a luminoimage analyzer (Fluor Chem Imaging System, Alpha Innotech Corporation, San Leandro, CA, USA).

Real-time reverse transcription (RT) PCR. The L4–L6 segment of the lumbar spinal cord and DRG were subjected to total RNA extraction according to the protocol of the manufacture and purified with QIAamp RNA Blood Mini (Qiagen, Valencia, CA, USA). The amount of total RNA concentration was measured using Smart Spec 3000 (Bio-Rad, Tokyo, Japan). Total RNA (175 ng) was converted to cDNA by reverse transcription, using random 9 mer (Takara, Otsu, Japan) and RNA PCR kit (Takara). The primers were as follows: CCL-1 primers (forward: 5′-TTCCCCTGAAGTTTATCCAGTGTT-3′, reverse: 5′-TGAACC CACGTTTTGTTAGTTGAG-3′); β-actin primers (forward: 5′-TTGCTGACAGGATG CAGAAGGAG-3′, reverse: 5′-GTGGACAGTGAGGCCAGGAT-3′); TNF-α primers (forward: 5′-CCACCACGCTCTTCTGTCTAC-3′, reverse: 5′-TGGGCTACAGGCTT GTCACT-3′); IL-1β primers (forward: 5′-CTCCATGAGCTTTGTACAAGG-3′, reverse: 5′-TGCTGATGTACCAGTTGGGG-3′); IL-6 primers (forward: 5′-ACACTC CTTAGTCCTCGGCCA-3′, reverse: 5′-CACGATTTCCCAGAGAACATGTG-3′); BDNF primers (forward: 5′-TGCAGGGGCATAGACAAAAGG-3′, reverse: 5′-CTTA TGAATCGCCAGCCAATTCTC-3′); Iba1 primers (forward: 5′-CCTGATTGGAGGT GGATGTCAC-3′, reverse: 5′-GGCTCACGACTGTTTCTTTTTTCC-3′); CD11b primers (forward: 5′-AATGATGCTTACCTGGGTTATGCT-3′, reverse: 5′-TGATAC CGAGGTGCTCCTAAAAC-3′); GFAP primers (forward: 5′-CCAGCTTCGAGCCAA GGA-3′, reverse: 5′-GAAGCTCCGCCTGGTAGACA-3′); and $P2X_4R$ primers (forward: 5′-TGGCCGACTATGTGGTCCCA-3′, reverse: 5′-GGTTCACGGTGACG ATCATG-3′). All primers were purchased from Sigma Aldrich Japan (Tokyo, Japan). PCR amplification was undertaken for Sybr qPCR Mix (Takara) in Applied Biosystems 7500 Real-Time PCR System (Applied Biosystems Japan, Tokyo, Japan). Each reaction volume consisted of 10 μl Sybr qPCR Mix, 0.4 μl 50 × ROX reference dye, 0.4 μl mix of forward and reverse primers (0.2 μM each) and 7.8 μl RNAase free water containing cDNA (17.5 ng). PCR was done by 15 s denaturation at 95 °C and annealing/extending at 60 °C for 40 cycles. Each mRNA expression level was normalized by β-actin. The mRNA expression was calculated relative to β-actin using the $\Delta\Delta C_T$ algorithm.

Western blotting. Expression protein level of CCR-8 in lumbar spinal cord was examined by western blotting relative to β-actin. The L4–L6 segments of the lumbar spinal cord were isolated and homogenized in a lysis buffer containing protease inhibitor (Sigma); subsequently 20 mg of proteins were loaded for each lane and separated by SDS-PAGE gel (7.5%), and transferred to PVDF membrane (Bio-Rad). The membrane was blocked with 5% low-fat dried milk (anti-CKR8/CCR-8), 5% BSA (anti-p-NR2B, anti-NR2B) or 3% BSA (anti-p-NR1, anti-NR1) and incubated with the following for 1 h at room temperature: Rabbit monoclonal anti-CKR8/CCR-8 (1 : 500, Epitomics, Burlingame, CA, USA), anti-phospho-NR1 (Ser896; 1 : 1000, Millipore), anti-NR1 (1 : 1000, Millipore), anti-phospho-NMDAR2B (Y1472; 1 : 1000, R&D Systems), anti-NMDAR2B (D15B3) (1 : 1000, Cell Signaling Technology), and anti-β-actin (1 : 1000, Sigma). The membrane was washed and incubated with specific secondary antibodies (Amersham ECL anti-rabbit IgG and anti-mouse IgG, horseradish peroxidase-linked species-specific whole antibody, 1 : 5000, GE Healthcare, Piscataway, NJ, USA). The blots were detected by use of ECL western blotting detection system (GE Healthcare) and LAS-4000 imaging system (Fujifilm, Tokyo, Japan). Bands were quantified using the software Multi Gauge (Fujifilm).

Preparation of spinal cord acute slices. The methods used for obtaining spinal cord slice preparations are identical to those described elsewhere.[53,54] Mice were anesthetized with urethane (1.2–1.5 g/kg, i.p.), and a thoracolumbar laminectomy was performed. The lumbosacral segments of the spinal cord (L1–S1) were placed in an ice-cold Krebs solution equilibrated with 95% O_2/5% CO_2. The Krebs solution contained (in mM) 117 NaCl, 3.6 KCl, 2.5 $CaCl_2$, 1.2 $MgCl_2$, 1.2 NaH_2PO_4, 25 $NaHCO_3$ and 11 glucose. Immediately after removal of the spinal cord, the mice were exsanguinated under the urethane anesthesia. The pia-arachnoid membrane was removed after cutting all of the ventral and dorsal roots. The spinal cord was mounted on a vibratome and a 500-μm thick transverse or sagittal slices were cut. The slice was placed on a nylon mesh in the recording chamber with a volume of 0.5 ml and was completely submerged and perfused with Krebs solution saturated with 95% O_2 and 5% CO_2 at 36 ± 1 °C at a flow rate of 10–15 ml/min.

Whole-cell patch-clamp recordings from substantia gelatinosa neurons. The substantia gelatinosa was easily discernible with transmitted illumination as a relatively translucent band across the dorsal horn in the transverse or parasagittal slice preparations. Blind whole-cell voltage-clamp recordings were made from SG neurons, as previously described.[53,54] The patch pipettes were filled with potassium gluconate solution, a solution containing (in mM); 135 K-gluconate, 5 KCl, 0.5 $CaCl_2$, 2 $MgCl_2$, 5 EGTA, 5 HEPES, and 5 ATP-Mg (pH 7.2). The tip resistance of the patch pipettes was 6–12 MΩ. Series resistance was assessed from current in response to a 5-mV hyperpolarizing step. Series resistance was monitored during the recording session and data were rejected if its value changed by > 15%. Ion currents were monitored with a patch-clamp amplifier (Axopatch 700A, Molecular Devices, Sunnyvale, CA, USA). The data were digitized with an analog-to-digital converter (Digidata 1321A, Molecular Devices), stored on a personal computer using a data acquisition program (Clampex version 10, Molecular Devices) and analyzed using a software package Clampfit version 10 (Molecular Devices). Recordings were made in a voltage-clamp mode at holding potential of − 70 mV to isolate EPSCs. Drugs were dissolved in the Krebs solution and applied by superfusion.

Transfection of CCR-8 siRNA by electroporation. siRNA against CCR-8 were obtained from Bonac Corporation (Kurume, Japan) (GenBank accession number: NM_007720, mCcr8#1 sense 5′-GCAAGAAACUGAGGAGCAU-3′, anti-sense 5′-AUGCUCCUCAGUUUCUUGC-3′, mCcr8#2 sense 5′-GAGCAGUC UUUGAGGUGGA-3′, anti-sense 5′-UCCACCUCAAAGACUGCUC-3′, and mCcr8#3 sense 5′-GAGAGAAGUUUAAGAAACA-3′, anti-sense 5′-UGUUUCUUAAACUUCU CUC-3′). Mice were anesthetized by pentobarbital sodium (50 mg/kg, i.p.). Mixed siRNA (0.2 μg/μl, 10 μl) was injected i.t. using a 25-μl Hamilton syringe with a 28-gauge needle (Muranaka Medical Instruments co. LTD.).[55,56] Scrambled siRNA (sense 5′-UACUAUUCGACACGCGAAG-3′, anti-sense 5′-CUUCGCGUGUCGAAUA-GUA-3′; Bonac Corporation) was used as a negative control. A volume of 5 μl was used for the i.t. injections at each points. Electric pulses (poring pulse: 75 V, 5 ms of length with 50-ms interval, transfer pulse: 20 V, 50 ms of length with 50-ms interval) were delivered using NEPA21 (Nepa Gene, Ichikawa, Japan).[57,58] Knock-down effects were evaluated by western blotting.

Cell culture. Cortex neurons were obtained from embryonic days 14–16 ddY mice as described previously.[59] Briefly, neurons were cultured at 37 °C in a 10% CO_2 incubator for 5–7 days with neurobasal medium (GIBCO, Grand Island, NY, USA) containing 2% B27 supplement (GIBCO) and 0.5 mM L-glutamine (GIBCO).

Immunocytochemical analysis. Primary cultured cells were fixed with 4% paraformaldehyde for 30 min at room temperature and permeabilized with 0.1% TritonX-100 in PBS for 5 min, followed by treating with blocking solution (Block Ace; Dainippon Pharmaceutical, Osaka, Japan) for 30 min at room temperature. Cells were incubated with primary antibodies: CCR-8 (1 : 200, Epitomics), MAP2 (1 : 1000, Sigma, St. Louis, MO, USA), VGLUT1 (1 : 1000, Synaptic Systems, Göttingen, Germany) or VGAT (1 : 500, Synaptic Systems) overnight at 4 °C. The cells were washed in PBS and then incubated for 3 h at room temperature with secondary antibody (IgG-conjugated Alexa Fluor 488 or 568 or 633, 1 : 1000, Molecular Probes). The cells were washed in PBS and treated with 4′, 6-diamidino-2-phenylindole (DAPI, 300 nM, Molecular Probes) for 10 min and then washed with PBS. Slides were cover-slipped with permafluor aqueous mounting medium. The sections were analyzed using a confocal laser scanning microscope (LSM510META, Carl Zeiss).

Statistical analysis. All data are presented as mean ± S.E.M. The statistical analyses of the results were evaluated by using two-tailed Student's paired or unpaired *t*-test, one-way ANOVA followed by Student–Newman–Keuls test, one-way ANOVA followed by Bonferroni's test or two-way ANOVA followed by Tukey–Kramer test. $P < 0.05$ was considered statistically significant.

Conflict of Interest

The authors declare no conflict of interest.

Acknowledgements. This work was supported, in part, by a Grant-in-Aid from the Ministry of Education, Culture, Sports, Science and Technology of Japan (No. 22590084 to MN, No. 22590252 to YT, No.23590731 to KH No. 23390156 to Dr. Hidemasa Furue and No. 5269 to NA). And this work was also supported by fund from the Central Research Institute of Fukuoka University. We appreciate the Research Support Center, Graduate School of Medical Sciences, Kyushu University for the technical support. We also thank Dr. Hidemasa Furue (National Institute for Physiological Sciences, Japan) for helping with the electrophysiological experiments, Professor Kazuhide Inoue and Dr. Hidetoshi Tozaki-Saitoh (Kyushu University) for an experimental equipment for behavioural test.

1. Woolf CJ, Mannion RJ. Neuropathic pain: aetiology, symptoms, mechanisms, and management. *Lancet* 1999; **353**: 1959–1964.
2. Inoue K, Tsuda M. Microglia and neuropathic pain. *Glia* 2009; **57**: 1469–1479.
3. Inoue K, Tsuda M, Koizumi S. ATP- and adenosine-mediated signaling in the central nervous system: chronic pain and microglia: involvement of the ATP receptor P2 × 4. *J Pharmacol Sci* 2004; **94**: 112–114.
4. Scholz J, Woolf CJ. The neuropathic pain triad: neurons, immune cells and glia. *Nat Neurosci* 2007; **10**: 1361–1368.
5. Petrenko AB, Yamakura T, Baba H, Shimoji K. The role of N-methyl-D-aspartate (NMDA) receptors in pain: a review. *Anesth Analg* 2003; **97**: 1108–1116.
6. Zhou HY, Chen SR, Pan HL. Targeting N-methyl-D-aspartate receptors for treatment of neuropathic pain. *Expert Rev Clin Pharmacol* 2011; **4**: 379–388.
7. Laube B, Kuhse J, Betz H. Evidence for a tetrameric structure of recombinant NMDA receptors. *J Neurosci* 1998; **18**: 2954–2961.
8. Lu WY, Jackson MF, Bai D, Orser BA, MacDonald JF. In CA1 pyramidal neurons of the hippocampus protein kinase C regulates calcium-dependent inactivation of NMDA receptors. *J Neurosci* 2000; **20**: 4452–4461.
9. Tingley WG, Ehlers MD, Kameyama K, Doherty C, Ptak JB, Riley CT *et al.* Characterization of protein kinase A and protein kinase C phosphorylation of the N-methyl-D-aspartate receptor NR1 subunit using phosphorylation site-specific antibodies. *J Biol Chem* 1997; **272**: 5157–5166.
10. Zou X, Lin Q, Willis WD. Enhanced phosphorylation of NMDA receptor 1 subunits in spinal cord dorsal horn and spinothalamic tract neurons after intradermal injection of capsaicin in rats. *J Neurosci* 2000; **20**: 6989–6997.
11. Milligan ED, Watkins LR. Pathological and protective roles of glia in chronic pain. *Nat Rev Neurosci* 2009; **10**: 23–36.
12. Thacker MA, Clark AK, Marchand F, McMahon SB. Pathophysiology of peripheral neuropathic pain: immune cells and molecules. *Anesth Analg* 2007; **105**: 838–847.
13. Calvo M, Dawes JM, Bennett DL. The role of the immune system in the generation of neuropathic pain. *Lancet Neurol* 2012; **11**: 629–642.
14. Ren K, Dubner R. Interactions between the immune and nervous systems in pain. *Nat Med* 2010; **16**: 1267–1276.
15. Dominguez E, Rivat C, Pommier B, Mauborgne A, Pohl M. JAK/STAT3 pathway is activated in spinal cord microglia after peripheral nerve injury and contributes to neuropathic pain development in rat. *J Neurochem* 2008; **107**: 50–60.
16. Tsuda M, Shigemoto-Mogami Y, Koizumi S, Mizokoshi A, Kohsaka S, Salter MW *et al.* P2 × 4 receptors induced in spinal microglia gate tactile allodynia after nerve injury. *Nature* 2003; **424**: 778–783.
17. Abbadie C, Bhangoo S, De Koninck Y, Malcangio M, Melik-Parsadaniantz S, White FA. Chemokines and pain mechanisms. *Brain Res Rev* 2009; **60**: 125–134.
18. Bajetto A, Bonavia R, Barbero S, Schettini G. Characterization of chemokines and their receptors in the central nervous system: physiopathological implications. *J Neurochem* 2002; **82**: 1311–1329.
19. Biber K, Vinet J, Boddeke HW. Neuron-microglia signaling: chemokines as versatile messengers. *J Neuroimmunol* 2008; **198**: 69–74.
20. Coyle DE. Partial peripheral nerve injury leads to activation of astroglia and microglia which parallels the development of allodynic behavior. *Glia* 1998; **23**: 75–83.
21. Luo Y, Laning J, Devi S, Mak J, Schall TJ, Dorf ME. Biologic activities of the murine beta-chemokine TCA3. *J Immunol* 1994; **153**: 4616–4624.
22. Tiffany HL, Lautens LL, Gao JL, Pease J, Locati M, Combadiere C *et al.* Identification of CCR8: a human monocyte and thymus receptor for the CC chemokine I-309. *J Exp Med* 1997; **186**: 165–170.
23. Gosselin RD, Suter MR, Ji RR, Decosterd I. Glial cells and chronic pain. *Neuroscientist* 2010; **16**: 519–531.
24. Biber K, Tsuda M, Tozaki-Saitoh H, Tsukamoto K, Toyomitsu E, Masuda T *et al.* Neuronal CCL21 up-regulates microglia P2 × 4 expression and initiates neuropathic pain development. *EMBO J* 2011; **30**: 1864–1873.
25. Jung H, Toth PT, White FA, Miller RJ. Monocyte chemoattractant protein-1 functions as a neuromodulator in dorsal root ganglia neurons. *J Neurochem* 2008; **104**: 254–263.
26. Van Steenwinckel J, Reaux-Le Goazigo A, Pommier B, Mauborgne A, Dansereau MA, Kitabgi P *et al.* CCL2 released from neuronal synaptic vesicles in the spinal cord is a major mediator of local inflammation and pain after peripheral nerve injury. *J Neurosci* 2011; **31**: 5865–5875.
27. Gao YJ, Ji RR. Targeting astrocyte signaling for chronic pain. *Neurotherapeutics* 2010; **7**: 482–493.
28. Miyoshi K, Obata K, Kondo T, Okamura H, Noguchi K. Interleukin-18-mediated microglia/astrocyte interaction in the spinal cord enhances neuropathic pain processing after nerve injury. *J Neurosci* 2008; **28**: 12775–12787.
29. Zhuang ZY, Gerner P, Woolf CJ, Ji RR. ERK is sequentially activated in neurons, microglia, and astrocytes by spinal nerve ligation and contributes to mechanical allodynia in this neuropathic pain model. *Pain* 2005; **114**: 149–159.
30. Smith JA, Das A, Ray SK, Banik NL. Role of pro-inflammatory cytokines released from microglia in neurodegenerative diseases. *Brain Res Bull* 2011; **87**: 10–20.
31. Beggs S, Trang T, Salter MW. P2X4R + microglia drive neuropathic pain. *Nat Neurosci* 2012; **15**: 1068–1073.
32. Kettenmann H, Hanisch UK, Noda M, Verkhratsky A. Physiology of microglia. *Physiol Rev* 2011; **91**: 461–553.
33. Guo LH, Schluesener HJ. Lesional accumulation of P2X(4) receptor(+) macrophages in rat CNS during experimental autoimmune encephalomyelitis. *Neuroscience* 2005; **134**: 199–205.
34. Verkhratsky A. Neuronismo y reticulismo: neuronal-glial circuits unify the reticular and neuronal theories of brain organization. *Acta Physiol (Oxf)* 2009; **195**: 111–122.
35. Beattie EC, Stellwagen D, Morishita W, Bresnahan JC, Ha BK, Von Zastrow M *et al.* Control of synaptic strength by glial TNFalpha. *Science* 2002; **295**: 2282–2285.
36. Fukuoka H, Kawatani M, Hisamitsu T, Takeshige C. Cutaneous hyperalgesia induced by peripheral injection of interleukin-1 beta in the rat. *Brain Res* 1994; **657**: 133–140.
37. Hou L, Li W, Wang X. Mechanism of interleukin-1 beta-induced calcitonin gene-related peptide production from dorsal root ganglion neurons of neonatal rats. *J Neurosci Res* 2003; **73**: 188–197.
38. Malcangio M, Bowery NG, Flower RJ, Perretti M. Effect of interleukin-1 beta on the release of substance P from rat isolated spinal cord. *Eur J Pharmacol* 1996; **299**: 113–118.
39. Zhang RX, Li A, Liu B, Wang L, Ren K, Zhang H *et al.* IL-1ra alleviates inflammatory hyperalgesia through preventing phosphorylation of NMDA receptor NR-1 subunit in rats. *Pain* 2008; **135**: 232–239.
40. Cui JG, Holmin S, Mathiesen T, Meyerson BA, Linderoth B. Possible role of inflammatory mediators in tactile hypersensitivity in rat models of mononeuropathy. *Pain* 2000; **88**: 239–248.
41. Fang XX, Jiang XL, Han XH, Peng YP, Qiu YH. Neuroprotection of interleukin-6 against NMDA-induced neurotoxicity is mediated by JAK/STAT3, MAPK/ERK, and PI3K/AKT signaling pathways. *Cell Mol Neurobiol* 2012; **33**: 241–251.
42. Ringheim GE, Burgher KL, Heroux JA. Interleukin-6 mRNA expression by cortical neurons in culture: evidence for neuronal sources of interleukin-6 production in the brain. *J Neuroimmunol* 1995; **63**: 113–123.
43. Liu XJ, Gingrich JR, Vargas-Caballero M, Dong YN, Sengar A, Beggs S *et al.* Treatment of inflammatory and neuropathic pain by uncoupling Src from the NMDA receptor complex. *Nat Med* 2008; **14**: 1325–1332.
44. Ultenius C, Linderoth B, Meyerson BA, Wallin J. Spinal NMDA receptor phosphorylation correlates with the presence of neuropathic signs following peripheral nerve injury in the rat. *Neurosci Lett* 2006; **399**: 85–90.
45. Gao X, Kim HK, Chung JM, Chung K. Enhancement of NMDA receptor phosphorylation of the spinal dorsal horn and nucleus gracilis neurons in neuropathic rats. *Pain* 2005; **116**: 62–72.
46. Abe T, Matsumura S, Katano T, Mabuchi T, Takagi K, Xu L *et al.* Fyn kinase-mediated phosphorylation of NMDA receptor NR2B subunit at Tyr1472 is essential for maintenance of neuropathic pain. *Eur J Neurosci* 2005; **22**: 1445–1454.
47. Guo W, Zou S, Guan Y, Ikeda T, Tal M, Dubner R *et al.* Tyrosine phosphorylation of the NR2B subunit of the NMDA receptor in the spinal cord during the development and maintenance of inflammatory hyperalgesia. *J Neurosci* 2002; **22**: 6208–6217.
48. Guo W, Wang H, Watanabe M, Shimizu K, Zou S, LaGraize SC *et al.* Glial-cytokine-neuronal interactions underlying the mechanisms of persistent pain. *J Neurosci* 2007; **27**: 6006–6018.
49. Seltzer Z, Dubner R, Shir Y. A novel behavioral model of neuropathic pain disorders produced in rats by partial sciatic nerve injury. *Pain* 1990; **43**: 205–218.
50. Honda K, Koga K, Moriyama T, Koguchi M, Takano Y, Kamiya HO. Intrathecal alpha2 adrenoceptor agonist clonidine inhibits mechanical transmission in mouse spinal cord via activation of muscarinic M1 receptors. *Neurosci Lett* 2002; **322**: 161–164.
51. Hylden JL, Wilcox GL. Intrathecal morphine in mice: a new technique. *Eur J Pharmacol* 1980; **67**: 313–316.
52. Gao YJ, Zhang L, Samad OA, Suter MR, Yasuhiko K, Xu ZZ *et al.* JNK-induced MCP-1 production in spinal cord astrocytes contributes to central sensitization and neuropathic pain. *J Neurosci* 2009; **29**: 4096–4108.
53. Yang K, Li Y, Kumamoto E, Furue H, Yoshimura M. Voltage-clamp recordings of postsynaptic currents in substantia gelatinosa neurons *in vitro* and its applications to assess synaptic transmission. *Brain Res Brain Res Protoc* 2001; **7**: 235–240.
54. Yoshimura M, Nishi S. Blind patch-clamp recordings from substantia gelatinosa neurons in adult rat spinal cord slices: pharmacological properties of synaptic currents. *Neuroscience* 1993; **53**: 519–526.

55. Morita K, Kitayama T, Morioka N, Dohi T. Glycinergic mediation of tactile allodynia induced by platelet-activating factor (PAF) through glutamate-NO-cyclic GMP signalling in spinal cord in mice. *Pain* 2008; **138**: 525–536.
56. Morita K, Motoyama N, Kitayama T, Morioka N, Kifune K, Dohi T. Spinal antiallodynia action of glycine transporter inhibitors in neuropathic pain models in mice. *J Pharmacol Exp Ther* 2008; **326**: 633–645.
57. Choijookhuu N, Sato Y, Nishino T, Endo D, Hishikawa Y, Koji T. Estrogen-dependent regulation of sodium/hydrogen exchanger-3 (NHE3) expression via estrogen receptor beta in proximal colon of pregnant mice. *Histochem Cell Biol* 2012; **137**: 575–587.
58. Yamano T, Iguchi H, Fukuzawa H. Rapid transformation of *Chlamydomonas reinhardtii* without cell-wall removal. *J Biosci Bioeng* 2012; **115**: 691–694.
59. Noda M, Kariura Y, Pannasch U, Nishikawa K, Wang L, Seike T *et al.* Neuroprotective role of bradykinin because of the attenuation of pro-inflammatory cytokine release from activated microglia. *J Neurochem* 2007; **101**: 397–410.

Supplementary Information accompanies this paper on Cell Death and Disease website (http://www.nature.com/cddis)

Effect of Allergen Sensitization on External Root Resorption

N. Murata, H. Ioi, M. Ouchi, T. Takao, H. Oida, R. Aijima, T. Yamaza and M.A. Kido

J DENT RES 2013 92: 641 originally published online 6 May 2013

DOI: 10.1177/0022034513488787

RESEARCH REPORTS
Biological

N. Murata[1,2], H. Ioi[2], M. Ouchi[1,2], T. Takao[1], H. Oida[1], R. Aijima[1], T. Yamaza[1], and M.A. Kido[1]*

[1]Department of Molecular Cell Biology and Oral Anatomy, Graduate School of Dental Science, Kyushu University, Fukuoka 812-8582, Japan; and [2]Department of Orthodontics, Graduate School of Dental Science, Kyushu University, Fukuoka, Japan; *corresponding author, kido@dent.kyushu-u.ac.jp

J Dent Res 92(7):641-647, 2013

Effect of Allergen Sensitization on External Root Resorption

ABSTRACT

In orthodontic tooth movement (OTM), we should be concerned about external root resorption (ERR) as an undesirable iatrogenic problem, but its mechanisms are not fully understood. Since our previous epidemiologic studies found that patients with allergic diseases showed higher rates of ERR during orthodontic treatment, we explored the possible effect of allergic sensitization on ERR. In ovalbumin (OVA)-sensitized Brown–Norway rats, the amounts of ERR and OTM were greater than those in animals subjected to orthodontic force alone. The expression levels of RANKL and pro-inflammatory cytokines were increased in the periodontal tissues of sensitized rats with OTM, compared with control rats. Furthermore, leukotriene B_4 (LTB_4), a potent lipid mediator of allergic inflammation, and enzymes of the 5-lipoxygenase pathway, the biosynthetic pathway of leukotrienes, were also up-regulated. We found that low doses of aspirin suppressed ERR in allergen-sensitized rats, as well as the expressions of RANKL, pro-inflammatory cytokines, and LTB_4. The present findings indicate that allergen sensitization has adverse effects on ERR under OTM, and that aspirin is a potential therapeutic agent for combating ERR.

KEY WORDS: allergy, tooth movement, cytokines, leukotrienes, aspirin, rats.

DOI: 10.1177/0022034513488787

Received November 14, 2012; Last revision March 13, 2013; Accepted April 10, 2013

A supplemental appendix to this article is published electronically only at http://jdr.sagepub.com/supplemental.

INTRODUCTION

Many orthodontists consider that undesirable external root resorption (ERR) is an unavoidable and unpredictable pathologic consequence of orthodontic tooth movement (OTM). Serious cases may involve shortening of the tooth roots, which in turn shortens the life of the tooth. This problem remains a matter of grave concern for orthodontic treatments. A few clinical reviews concerning ERR have suggested the involvement of systemic conditions, including allergic conditions (McNab *et al.*, 1999; Davidovitch *et al.*, 2000). Indeed, we previously showed that Japanese patients with allergic diseases had higher rates of orthodontically induced root resorption (Nishioka *et al.*, 2006). However, the mechanisms of ERR under allergic conditions are still poorly understood.

Pro-inflammatory cytokines, such as tumor necrosis factor (TNF)-α and interleukin (IL)-1β, and receptor activator of nuclear factor κB ligand (RANKL) play well-known roles in bone resorption through the induction of osteoclast differentiation (Heath *et al.*, 1985; Bertolini *et al.*, 1986), and have been suggested to be involved in OTM (Lowney *et al.*, 1995; Kanzaki *et al.*, 2002). TNF-α and IL-1β induce local expression of RANKL, which is critical for the terminal differentiation of osteoclast precursor cells (Suda *et al.*, 1999; Azuma *et al.*, 2000). Furthermore, leukotrienes, which are metabolites of arachidonic acid, are potent lipid mediators that play important roles in allergic inflammation and constitute several products of the 5-lipoxygenase (5-LOX) pathway (Murphy and Gijon, 2007). Increased levels of leukotrienes are found in inflammatory diseases such as asthma and periodontal diseases (Emingil *et al.*, 2001; Hallstrand and Henderson, 2010). Hikiji *et al.* (2009) reported that leukotriene B_4 (LTB_4) modulates bone metabolism by increasing bone resorption. These LTB_4 actions are mediated by specific receptors, BLT1 and BLT2 (Yokomizo *et al.*, 1997, 2000).

Brown–Norway (BN) rats, which spontaneously produce high levels of serum IgE and show further highly enhanced serum IgE levels after sensitization with ovalbumin (OVA), have been extensively used as animal models of asthma (Bellofiore and Martin, 1988) and atopic dermatitis (Imada *et al.*, 2002).

To explore the possibility that allergies increase OTM and ERR, we examined the effects of allergen sensitization on ERR and OTM using OVA-sensitized BN rats. Furthermore, we attempted to prevent ERR progression during OTM by aspirin administration, since aspirin has been reported to improve bone mineral density in human epidemiological studies (Bauer *et al.*, 1996; Carbone *et al.*, 2003).

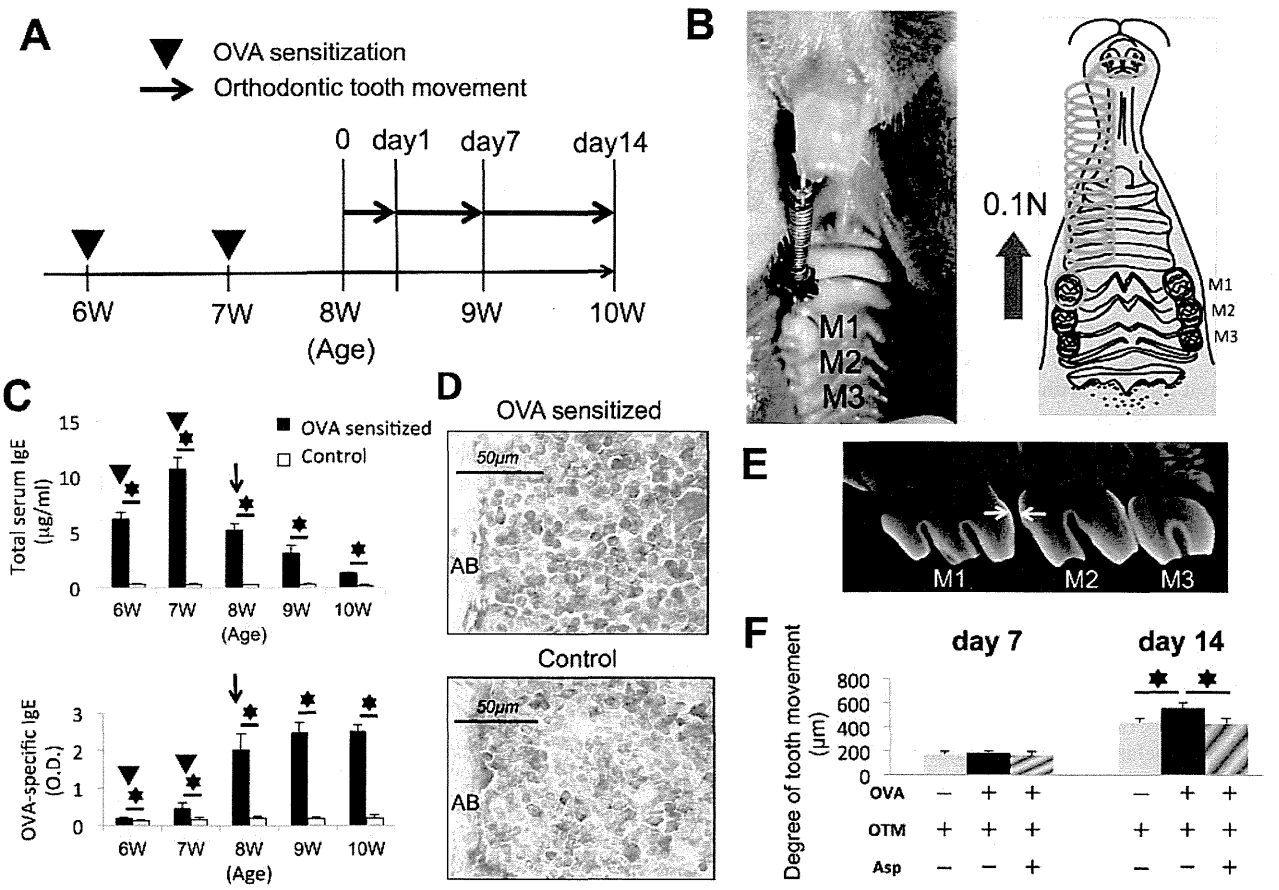

Figure 1. Experimental design, changes in serum IgE, histology of alveolar bone, and degrees of tooth movement. **(A)** Scheme showing the experimental design regarding OVA sensitization, orthodontic force application, and aspirin administration. **(B)** Photomicrograph and scheme of rat maxillae with the orthodontic appliance. The force level of the closed-coil spring after activation is approximately 0.1 N. M1, first molar; M2, second molar; M3, third molar. **(C)** The total and OVA-specific IgE levels in serum are greatly elevated after the first OVA sensitization, and further elevated after the second OVA sensitization. The arrowheads indicate the times of the 2 OVA sensitizations. The arrows indicate the start of the orthodontic force application. All data are expressed as means ± SD. *$p < .05$ by Student's *t* test (n = 7 animals *per* group). **(D)** Granulocytes including eosinophils are increased in OVA-sensitized alveolar bone marrow compared with control alveolar bone marrow. The sections are stained with Giemsa. AB, alveolar bone. **(E)** Micro-CT photograph showing the maxilla from a rat in the OVA with OTM group. The arrows indicate the dissociation of tooth movement. **(F)** The degree of tooth movement is significantly greater in OVA-sensitized animals than in non-sensitized animals after tooth movement. Aspirin treatment reverses the increase in OVA-sensitized animals. All data are expressed as means ± SD. *$p < .05$ by one-way ANOVA with Tukey's multiple-comparison test (n = 7 animals *per* group).

MATERIALS & METHODS

Rats

The experimental protocols were approved by the Animal Care and Use Committee of Kyushu University. Six-week-old male BN rats (Kyudo, Tosu, Japan) weighing 110 to 140 g were fed a powdered diet (CE-2; Clea Japan, Tokyo, Japan) and given water *ad libitum*.

Allergen Sensitization

The rats were sensitized by a subcutaneous injection of saline (1 mL) containing 1 mg of OVA (grade V; Sigma-Aldrich, St. Louis, MO, USA) and 200 mg of aluminum hydroxide. A *Bordetella pertussis* vaccine containing 1×10^{10} heat-killed bacilli (Wako, Osaka, Japan) was given intraperitoneally as an adjuvant, and OVA was injected after 7 days. ELISAs were used to detect total serum IgE (Shibayagi, Gunma, Japan) and OVA-specific IgE (Cusabio, Newark, DE, USA) in the OVA-alone and control groups (n = 7 *per* group).

OTM and Aspirin Administration

At 7 days after the second sensitization, an Ni-Ti closed-coil spring at a force of 0.1 N (Sentalloy®, Ultra Light; Tomy International Inc., Tokyo, Japan) was inserted between the upper right first molar (M1) and the incisors (Figs. 1A, 1B).

Aspirin dissolved in feed water (250 μg/kg/day) was administered to OVA-sensitized rats at the time of orthodontic force application. For ELISA and RT-PCR analyses, aspirin was administered from 24 hrs before OTM.

The animals were divided into 5 groups: control group (no OVA or OTM); OVA-alone group (no OTM); OTM-alone group (no OVA); 'OVA with OTM' group; and 'aspirin administration

to OVA with OTM' group. We used separate animals for the different analyses.

Histology

After 7 and 14 days of OTM, the animals (n = 7 *per* group) were perfused transcardially with 200 mL of heparinized phosphate-buffered saline, pH 7.4, followed by 4% paraformaldehyde containing 0.2% picric acid in 0.1 M phosphate buffer. The right halves of maxillae decalcified in 10% EDTA were cut into 8-μm-thick parasagittal sections, and every fifth section was collected. The sections showing the greatest length of the disto-palatal root together with the 5 adjacent sections on either side (total of 11 sections *per* animal) were stained for tartrate-resistant acid phosphatase (TRAP) (Sigma-Aldrich) or Giemsa (Merck, Darmstadt, Germany). All sections were observed under a digital microscope with MZ-II Analyzer software (BZ-9000; Keyence, Osaka, Japan).

After investigation of all 5 roots of M1 with surrounding structures, we found that ERR was conspicuous in the distopalatal root. We measured the area of ERR as well as the numbers of odontoclasts and osteoclasts within a defined area (Appendix Fig. 1) according to the method of Mavragani *et al.* (2005). The resorption area (eroded surface *per* bone surface; ES/BS) and adjacent osteoclasts (osteoclast number *per* bone surface; N.Oc/BS) were also measured in the adjacent alveolar bone. We counted TRAP-positive cells in resorption lacunae facing the tooth roots as odontoclasts, and other TRAP-positive cells (containing more than 2 nuclei) as osteoclasts.

Cytokines and Leukotriene

The periodontal tissues, including the bone, surrounding M1 of the right maxillae after 24 hrs of OTM (n = 7 *per* group) were immediately frozen in liquid nitrogen and homogenized in Tris-HCl buffer, pH 7.4, containing protease inhibitors. After centrifugation, the supernatants were collected and stored at −80°C. TNF-α, IL-1β, and IL-6 were evaluated with a TNF-α ELISA Kit (Shibayagi), an IL-1β ELISA Kit, and an IL-6 ELISA Kit (BioSource, Camarillo, CA, USA), respectively, according to the manufacturers' protocols.

Lipid was extracted in 100% methanol at −30°C overnight, and the level was evaluated with an EIA Kit (Cayman Chemical, Ann Arbor, MI, USA).

RT-PCR

The periodontal tissues around M1 after 24 hrs of OTM were rapidly frozen in liquid nitrogen and homogenized (n = 4 *per* group). After mRNA isolation, quantitative real-time PCR or conventional RT-PCR was performed with gene-specific primer sets (Appendix Table), as described previously (Wang *et al.*, 2011). Amplification for real-time PCR was performed with a Rotor Gene 3000 (QIAGEN K.K., Tokyo, Japan). All samples were normalized by the expression of glyceraldehyde-3-phosphate dehydrogenase or 18S ribosomal RNA.

Micro-CT

Micro-CT images were acquired at 9-μm resolution with a SkyScan 1076 (SkyScan, Antwerp, Belgium) used to assess the degree of OTM. At day 14 (10 wks of age), the hemi-maxillae were excised (n = 6 *per* group). The hemi-maxilla samples were directed parallel to the occlusal plane and scanned for 2.70 mm. The distance from the distal surface of M1 to the mesial surface of the second molar (M2) was measured with DataViewer software (ver. 1.4.3; SkyScan).

Statistical Analysis

The serum IgE levels were compared by Student's *t* test. The means of multiple groups were compared by one-way analysis of variance (ANOVA). Other values were compared by ANOVA followed by Tukey's multiple-comparison test. Values of $p < .05$ were considered to indicate statistical significance.

RESULTS

Systemic and Local Changes with OVA Sensitization

The total serum IgE and OVA-specific IgE levels were greatly elevated after the first OVA sensitization, and further elevated after the second sensitization (Fig. 1C). Interestingly, the numbers of granulocytes including eosinophils were increased in the alveolar bone marrow at 7 days after the second OVA sensitization compared with those in non-sensitized control alveolar bone marrow (Fig. 1D). Acute lung inflammation was confirmed by intranasal OVA challenge (Appendix Fig. 2).

To explore whether allergen sensitization had specific effects on only the alveolar bone with OTM or systemic effects on the long bones as well, we examined the proximal metaphyseal region of the tibia using micro-CT. There were no significant differences in the bone structural parameters between the groups (Appendix Fig. 3).

The body weights showed no significant differences among the groups (Appendix Fig. 4).

OTM and Root and Alveolar Bone Resorption

At day 14, the degree of OTM was significantly larger in the 'OVA with OTM' group than in the OTM-alone group (Fig. 1E). Without orthodontic force, no osteoclasts and/or odontoclasts were observed on the medial surface of the alveolar bone in any of the groups (Figs. 2A–2E). Marked ERR was observed on the pressured side in the OTM-alone and 'OVA with OTM' groups (Figs. 2C, 2D). The 'OVA with OTM' group exhibited broad and deep TRAP-stained areas, with resorption lacunae on the root and surrounding bone on days 7 and 14 (Figs. 2D, 2F). In addition, the numbers of odontoclasts and osteoclasts were significantly greater in the 'OVA with OTM' group than in the OTM-alone group (Figs. 2G, 2H). The number of osteoclasts peaked on day 7 in the 'OVA with OTM' group, and then decreased by day 14. While the area of ERR increased from day 7 to day 14, the number of odontoclasts was maintained during this period (Figs. 2F, 2H). The alveolar bone resorption and osteoclast numbers were significantly greater in the

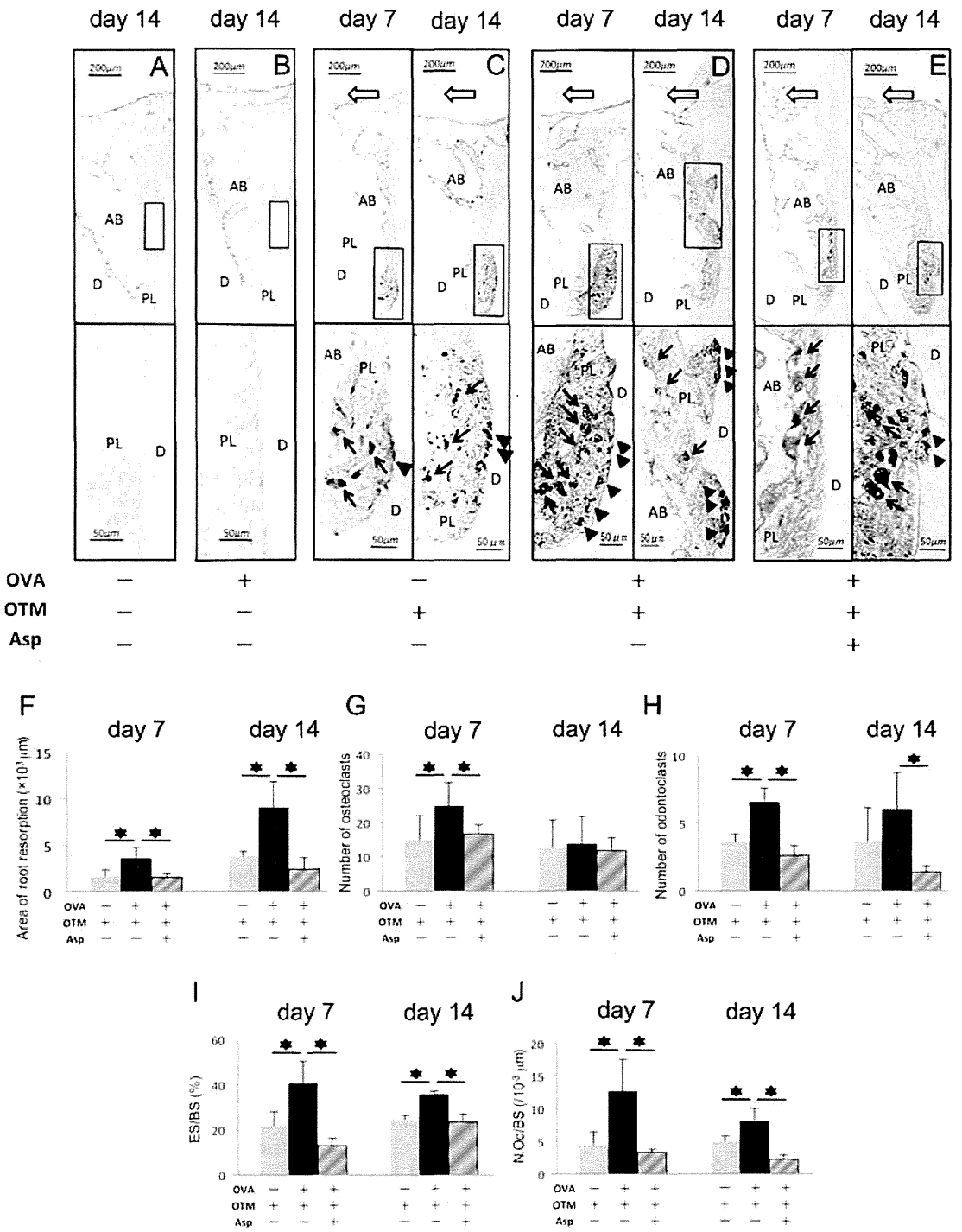

Figure 2. Increased numbers of osteoclasts/odontoclasts and amounts of root/bone resorption on the pressured side after tooth movement in OVA-sensitized animals, and inhibition of these increases by aspirin administration. Histologic sections of periodontal tissues around the distopalatal root of the first molar stained for TRAP after 7 and 14 days of tooth movement **(A–E)** and quantitative analyses **(F–J).** The upper panels show low-magnification images and the lower panels show high-magnification images of the boxed areas in the upper panels. **(A)** Control group (without treatment). **(B)** OVA-alone group. **(C)** OTM-alone group. **(D)** 'OVA with OTM' group. **(E)** 'Aspirin administration to OVA with OTM' group. **(F)** Area of root resorption ($\times 10^3$ μm^2). **(G)** Number of osteoclasts. **(H)** Number of odontoclasts. **(I)** Eroded surface *per* alveolar bone surface (ES/BS). **(J)** Number of osteoclasts *per* alveolar bone surface (N.Oc/BS). The white arrows indicate the orthodontic force direction. The black arrows indicate TRAP-positive osteoclasts. The arrowheads indicate TRAP-positive odontoclasts. The sections are counterstained with toluidine blue. AB, alveolar bone; D, dentin; PL, periodontal ligament. All data are expressed as means ± SD. $*p < .05$ by one-way ANOVA with Tukey's multiple-comparison test (n = 7 animals *per* group).

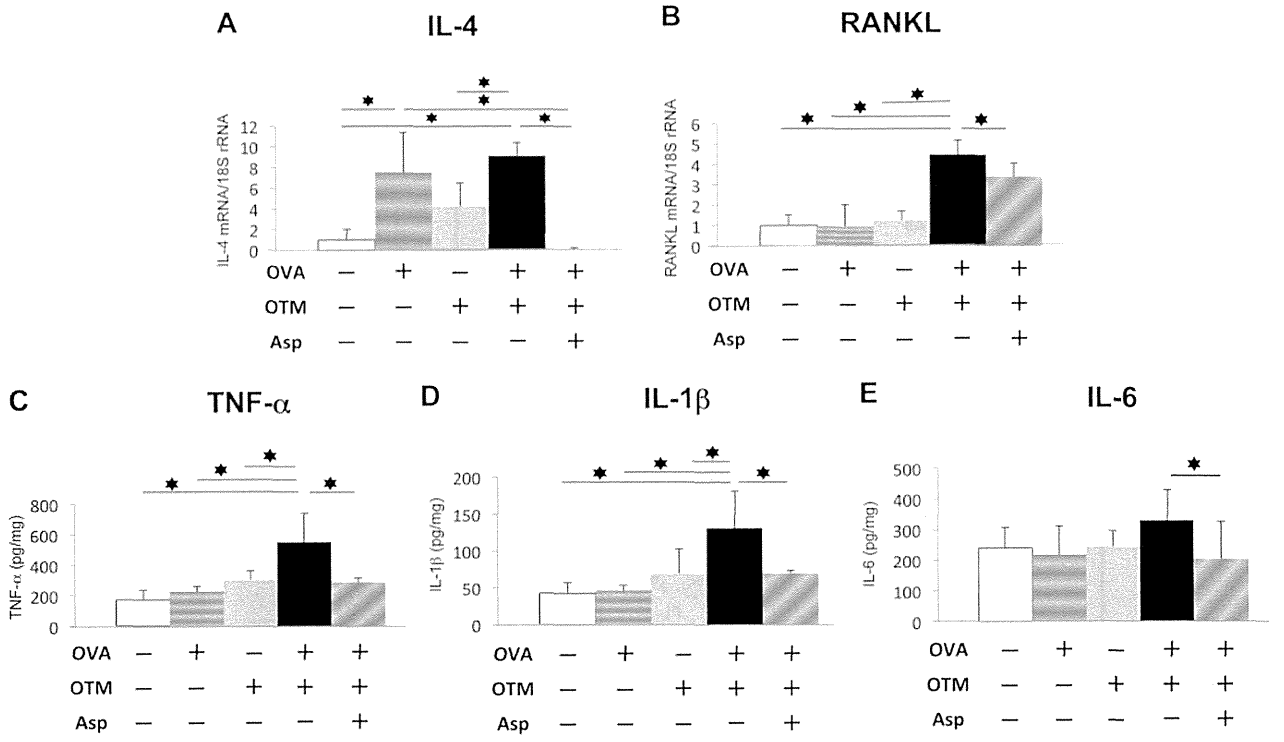

Figure 3. Elevated expressions of cytokines in periodontal tissues after 24 hrs of tooth movement in OVA-sensitized animals, and suppression of these elevations by aspirin administration. **(A)** IL-4. **(B)** RANKL. **(C)** TNF-α. **(D)** IL-1β. **(E)** IL-6. All data are expressed as means ± SD. *$p < .05$ by one-way ANOVA with Tukey's multiple-comparison test (n = 7 animals *per* group).

'OVA with OTM' group than in the OTM-alone group on days 7 and 14 (Figs. 2I, 2J).

Cytokines

To identify the possible mechanism for the elevated ERR, we examined the levels of cytokines in the periodontal tissues surrounding M1 after 24 hrs of OTM. The IL-4 level was significantly higher in the OVA-alone and 'OVA with OTM' groups than in the control group (Fig. 3A). The levels of RANKL, TNF-α, and IL-1β were significantly higher in the 'OVA with OTM' group than in the other groups (Figs. 3B–3D), while the difference in IL-6 was not significant (Fig. 3E). Although there were no significant differences between the OVA-alone and control groups, the OTM-alone group showed tendencies toward higher levels of TNF-α and IL-1β (Figs. 3C, 3D).

LTB_4 and Related Factors

The LTB_4 level and mRNA levels of the synthases 5-LOX and LTA_4 hydrolase (LTA_4h) were significantly higher in the 'OVA with OTM' group than in the other groups after 24 hrs of OTM (Figs. 4A–4C, 4F). The mRNA levels of the LTB_4 receptors BLT1 and BLT2 were also higher in the 'OVA with OTM' group (Figs. 4D–4F).

Effects of Aspirin Administration

Aspirin treatment reversed the degree of OTM in the 'OVA with OTM' group to a level similar to that in the OTM-alone group on day 14 (Fig. 1E). Histologic examinations revealed that the area of ERR and numbers of odontoclasts/osteoclasts were decreased to the levels observed in the OTM-alone group (Figs. 2E–2J). The levels of IL-4 and RANKL mRNAs, and TNF-α, IL-1β, and IL-6 proteins were also suppressed to the levels detected in the OTM-alone group (Fig. 3). Furthermore, the amounts of LTB_4, BLT1, BLT2, 5-LOX, and LTA_4h were also suppressed by aspirin treatment (Fig. 4).

DISCUSSION

The main findings of the present study are that the amounts of OTM, alveolar bone resorption, and ERR appear to be associated with systemic allergen sensitization. The increased numbers of odontoclasts/osteoclasts on the pressured side during OTM in OVA-sensitized rats, suggesting odontoclastogenesis/osteoclastogenesis under the condition of orthodontic force, were stimulated by systemic allergen sensitization. Since we observed these changes in maxillae after OVA sensitization (under high serum IgE conditions) without further OVA challenge to the skin or nose, the allergic background may be associated with susceptibility to ERR. These findings may support the idea that allergic diseases affect OTM, which was raised by our previous epidemiologic observations showing increased rates of ERR in patients with allergic diseases (Nishioka *et al.*, 2006).

We found markedly elevated serum IgE and OVA-specific IgE levels and, at the same time, observed increased infiltration of inflammatory granulocytes and IL-4 mRNA levels in the periodontal tissue. These findings suggest that OVA sensitization stimulates

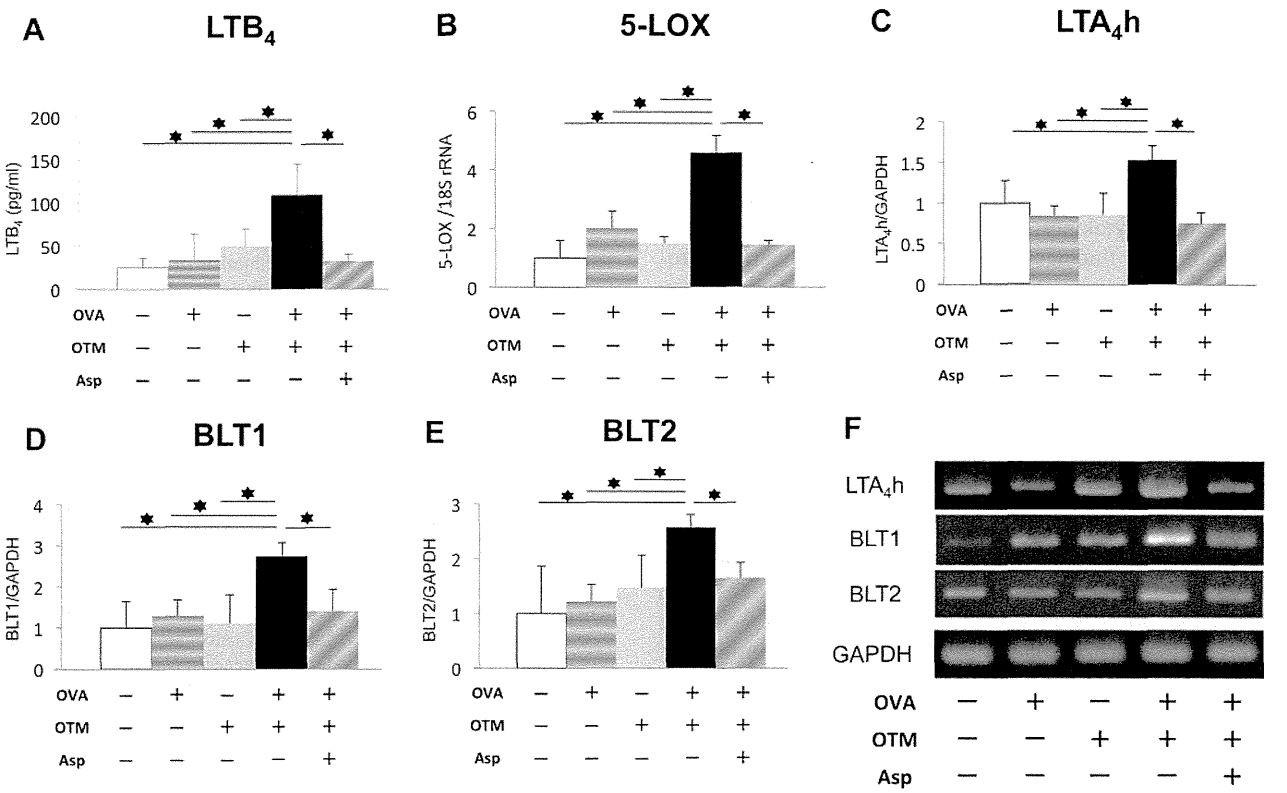

Figure 4. Augmentation of LTB_4 levels and mRNA levels of LTB_4 synthases and receptors in periodontal tissues after 24 hrs of tooth movement in OVA-sensitized animals, and inhibition of these elevations by aspirin administration. **(A)** Concentration of LTB_4 in periodontal tissues. **(B–F)** mRNA levels of leukotriene synthases and receptors determined by real-time **(B)** and conventional **(C–F)** RT-PCR. The mRNA levels of the leukotriene synthases 5-LOX **(B)** and LTA_4h **(C)**, and BLT1 **(D)** and BLT2 **(E)** and the electrophoretograms **(F)** are shown. All data are expressed as means ± SD. $*p < .05$ by one-way ANOVA with Tukey's multiple-comparison test (n = 4 animals *per* group).

IL-4 production, consistent with a previous report (Renzi *et al.*, 1996). Furthermore, higher expressions of TNF-α and IL-1β, well-known pro-inflammatory cytokines, were detected in the periodontal tissues of the 'OTM with OVA' group. Recently, Polzer *et al.* (2011) reported that TNF-α-transgenic IL-1β-deleted mice were protected against bone loss, suggesting that IL-1β contributes to TNF-α-mediated inflammatory osteopenia. The elevated levels of TNF-α and IL-1β, together with RANKL as an essential cytokine for osteoclastogenesis, suggest increased rates and magnitudes of ERR and OTM for the differentiation of odontoclasts/osteoclasts. IL-4 is known to suppress TNF-α and RANKL-mediated osteoclast formation *in vitro* (Kong *et al.*, 1999; Kitaura *et al.*, 2003) and *in vivo* (Fujii *et al.*, 2012), while mice overexpressing IL-4 develop systemic bone loss (Lewis *et al.*, 1993). In the periodontal tissues of allergen-sensitized animals, clarification of the cytokines that cause the exacerbation of tooth or bone resorption requires further studies.

Leukotrienes have been implicated in bone remodeling in several reports. Garcia *et al.* (1996) showed that LTB_4 stimulated osteoclastic bone resorption, and Hikiji *et al.* (2009) demonstrated that bone resorption was attenuated in ovariectomized BLT1-knockout mice. We observed higher levels of LTB_4 together with increased expressions of the receptors BLT1 and BLT2, as well as 5-LOX and LTA_4h, biosynthetic enzymes for leukotrienes, suggesting enhanced production of LTB_4 in the tissues during OTM with allergic inflammation. Based on these findings, the elevated expressions of LTB_4 and its receptors together with the pro-inflammatory cytokines TNF-α and IL-1β may augment the ERR and OTM through RANKL-mediated osteoclastogenesis. It can be considered that the reciprocal induction of the leukotriene pathway and pro-inflammatory cytokines is involved in the mechanisms of ERR and OTM.

Elderly men and women taking aspirin were reported to show higher bone mineral density than non-takers (Carbone *et al.*, 2003). Yamaza *et al.* (2008) showed that low-dose aspirin inhibited ovariectomy-induced osteoporosis by inhibiting T-cell activation in mice. Administration of aspirin at much lower doses than for general use as a painkiller was able to reverse the increases in ERR, degrees of OTM, and the levels of leukotriene signaling pathway components in our allergen-sensitized model. These findings raise the possibility that low-dose aspirin administration inhibits osteoclastogenesis under inflammatory conditions through the production of anti-inflammatory lipid mediator resolvins (Bento *et al.*, 2011). In our limited experimental period, we did not find that allergy affected the bone structural parameters of the tibia. However, repeated sensitization with allergens over a longer period suggested effects on bone metabolism (unpublished observations). Thus, the increased degree of OTM could be caused by alterations in the structural properties of alveolar bone as well as the enhanced osteoclastogenesis. For

further understanding of the complexity and diversity of molecules associated with the regulation of root and alveolar bone resorption with allergic inflammation, both systemic and locoregional experiments are needed.

In conclusion, we have proposed a model for studying the effects of allergen-induced inflammation and/or mechanical stress on ERR during OTM. This process was affected by pro-inflammatory cytokines, together with lipid mediators. Furthermore, our findings suggest that pro-inflammatory cytokines and leukotrienes, together with low-dose aspirin, may represent pharmacological targets for ERR during orthodontic treatment with allergic conditions.

ACKNOWLEDGMENTS

We thank Dr. I. Takahashi for valuable advice. We appreciate the technical support from the Research Support Center, Graduate School of Medical Sciences, Kyushu University. This study was supported by a Grant-in-Aid for Scientific Research (C) (to H.I.) and by a Grant-in-Aid for Young Scientists (B) (to N.M.) from the Japanese Ministry of Education, Culture, Sports, Science and Technology. The authors declare no potential conflicts of interest with respect to the authorship and/or publication of this article.

REFERENCES

Azuma Y, Kaji K, Katogi R, Takeshita S, Kudo A (2000). Tumor necrosis factor-alpha induces differentiation of and bone resorption by osteoclasts. *J Biol Chem* 275:4858-4864.

Bauer DC, Orwoll ES, Fox KM, Vogt TM, Lane NE, Hochberg MC, *et al.* (1996). Aspirin and NSAID use in older women: effect on bone mineral density and fracture risk. *J Bone Miner Res* 11:29-35.

Bellofiore S, Martin JG (1988). Antigen challenge of sensitized rats increases airway responsiveness to methacholine. *J Appl Physiol* 65:1642-1646.

Bento AF, Claudino RF, Dutra RC, Marcon R, Calixto JB (2011). Omega-3 fatty acid-derived mediators 17(R)-hydroxy docosahexaenoic acid, aspirin-triggered resolvin D1 and resolvin D2 prevent experimental colitis in mice. *J Immunol* 187:1957-1969.

Bertolini DR, Nedwin GE, Bringman TS, Smith DD, Mundy GR (1986). Stimulation of bone resorption and inhibition of bone formation in vitro by human tumour necrosis factors. *Nature* 319:516-518.

Carbone LD, Tylavsky FA, Cauley JA, Harris TB, Lang TF, Bauer DC, *et al.* (2003). Association between bone mineral density and the use of nonsteroidal anti-inflammatory drugs and aspirin: impact of cyclooxygenase selectivity. *J Bone Miner Res* 18:1795-1802.

Davidovitch Z, Lee XJ, Counts AL, Park YG (2000). The immune system possibly modulates orthodontic root resorption. In: Biological mechanisms of tooth movement and craniofacial adaptation. Davidovitch Z, Mah J, editors. Boston, MA: Harvard Society for the Advancement of Orthodontics, pp. 207-217.

Emingil G, Cinarcik S, Baylas H, Coker I, Huseyinov A (2001). Levels of leukotriene B4 in gingival crevicular fluid and gingival tissue in specific periodontal diseases. *J Periodontol* 72:1025-1031.

Fujii T, Kitaura H, Kimura K, Hakami ZW, Takano-Yamamoto T (2012). IL-4 inhibits TN F-α-mediated osteoclast formation by inhibition of RANKL expression in TNF-α-activated stromal cells and direct inhibition of TNF-α-activated osteoclast precursors via a T-cell-independent mechanism in vivo. *Bone* 51:771-780.

Garcia C, Boyce BF, Gilles J, Dallas M, Qiao M, Mundy GR, *et al.* (1996). Leukotriene B4 stimulates osteoclastic bone resorption both in vitro and in vivo. *J Bone Miner Res* 11:1619-1627.

Hallstrand TS, Henderson WR Jr (2010). An update on the role of leukotrienes in asthma. *Curr Opin Allergy Clin Immunol* 10:60-66.

Heath JK, Saklatvala J, Meikle MC, Atkinson SJ, Reynolds JJ (1985). Pig interleukin 1 (catabolin) is a potent stimulator of bone resorption in vitro. *Calcif Tissue Int* 7:95-97.

Hikiji H, Ishii S, Yokomizo T, Takato T, Shimizu T (2009). A distinctive role of the leukotriene B4 receptor BLT1 in osteoclastic activity during bone loss. *Proc Natl Acad Sci USA* 106:21294-21299.

Imada T, Komorita N, Kobayashi F, Naito K, Yoshikawa T, Miyazaki M, *et al.* (2002). Therapeutic potential of a specific chymase inhibitor in atopic dermatitis. *Jpn J Pharmacol* 90:214-217.

Kanzaki H, Chiba M, Shimizu Y, Mitani H (2002). Periodontal ligament cells under mechanical stress induce osteoclastogenesis by receptor activator of nuclear factor kappaB ligand up-regulation via prostaglandin E2 synthesis. *J Bone Miner Res* 17:210-220.

Kitaura H, Nagata N, Fujimura Y, Hotokezaka H, Tatamiya M, Nakao N, *et al.* (2003). Interleukin-4 directly inhibits tumor necrosis factor-alpha-mediated osteoclast formation in mouse bone marrow macrophages. *Immunol Lett* 88:193-198.

Kong YY, Yoshida H, Sarosi I, Tan HL, Timms E, Capparelli C, *et al.* (1999). OPGL is a key regulator of osteoclastogenesis, lymphocyte development and lymph-node organogenesis. *Nature* 397:315-323.

Lewis DB, Liggitt HD, Effmann EL, Motley ST, Teitelbaum SL, Jepsen KJ, *et al.* (1993). Osteoporosis induced in mice by overproduction of interleukin 4. *Proc Natl Acad Sci USA* 90:11618-11622.

Lowney JJ, Norton LA, Shafer DM, Rossomando EF (1995). Orthodontic forces increase tumor necrosis factor alpha in the human gingival sulcus. *Am J Orthod Dentofacial Orthop* 108:519-524.

Mavragani M, Brudvik P, Selvig KA (2005). Orthodontically induced root and alveolar bone resorption: inhibitory effect of systemic doxycycline administration in rats. *Eur J Orthod* 27:215-225.

McNab S, Battistutta D, Taverne A, Symons AL (1999). External apical root resorption of posterior teeth in asthmatics after orthodontic treatment. *Am J Orthod Dentofacial Orthop* 116:545-551.

Murphy RC, Gijon MA (2007). Biosynthesis and metabolism of leukotrienes. *Biochem J* 405:379-395.

Nishioka M, Ioi H, Nakata S, Nakasima A, Counts A (2006). Root resorption and immune system factors in the Japanese. *Angle Orthod* 76:103-108.

Polzer K, Neubert K, Meister S, Frey B, Baum W, Distler JH, *et al.* (2011). Proteasome inhibition aggravates TNF-mediated bone resorption. *Arthritis Rheum* 63:670-680.

Renzi PM, al Assaad AS, Yang J, Yasruel Z, Hamid Q (1996). Cytokine expression in the presence or absence of late airway responses after antigen challenge of sensitized rats. *Am J Respir Cell Mol Biol* 15:367-373.

Suda T, Takahashi N, Udagawa N, Jimi E, Gillespie MT, Martin TJ (1999). Modulation of osteoclast differentiation and function by the new members of the tumor necrosis factor receptor and ligand families. *Endocr Rev* 20:345-357.

Wang B, Danjo A, Kajiya H, Okabe K, Kido MA (2011). Oral epithelial cells are activated *via* TRP channels. *J Dent Res* 90:163-167.

Yamaza T, Miura Y, Bi Y, Liu Y, Akiyama K, Sonoyama W, *et al.* (2008). Pharmacologic stem cell based intervention as a new approach to osteoporosis treatment in rodents. *PLoS One* 3:e2615.

Yokomizo T, Izumi T, Chang K, Takuwa Y, Shimizu T (1997). A G-protein-coupled receptor for leukotriene B4 that mediates chemotaxis. *Nature* 387:620-624.

Yokomizo T, Kato K, Terawaki K, Izumi T, Shimizu T (2000). A second leukotriene B(4) receptor, BLT2. A new therapeutic target in inflammation and immunological disorders. *J Exp Med* 192:421-432.

神経生理検査

誘発電位検査を中心に

Point

- 多発性硬化症（MS）では，MRIで描出されない潜在性病変の検出に誘発電位検査が補助診断として有用である．
- MSの臨床で活用されている主な生理学的検査には視覚誘発電位，体性感覚誘発電位，運動誘発電位検査がある．
- 複数の誘発電位検査を組み合わせることによりMS病変の空間的多発性の証明に役立つ．

MSにおける神経生理検査

多発性硬化症（multiple sclerosis：MS）でよく用いられる神経生理検査は誘発電位検査である．MSは空間的多発性病変を特徴とするが，臨床症状や神経学的所見から病変部位を推定しながらも，MRIでは明らかな病変が描出されないことは日常の診療でしばしば経験される．それは，MRIが組織学的な変化を表すにすぎず，必ずしも機能的変化を反映していないことに起因している．誘発電位検査はこうしたMRIでは描出されない病変の証明において不可欠な存在である．また，明らかな臨床徴候を伴わない潜在性病変の検出にも優れており，MRIと併用することにより空間的多発性病変の証明に大きく寄与する．MSの臨床でよく用いられる誘発電位検査には，視覚誘発電位（visual evoked potential：VEP），体性感覚誘発電位（somatosensory evoked potential：SEP），運動誘発電位（motor evoked potential：MEP）がルーチン化されている．

視覚誘発電位（VEP）

VEPはMSによる視神経炎を診断する目的で行われる．視神経炎はMSを特徴づける臨床症状の一つであるが，通常の撮影条件のMRIでは異常を検出し得ないことがしばしばであり，視機能障害の程度とMRI所見の間には必ずしも相関がないことが多い．また，通常の視力・視野検査で異常がない場合においても，VEPにより潜在的な視神経の機能的障害を確認できることがあり（**1**），VEPはMSの診断の過程において欠かすことのできない検査である[1]．脊髄炎で初発する場合のclinically isolated syndromeや，MS以外の疾患の検査目的で施行されたMRIで偶然MS様病変が見つかった場合（radiologically isolated syndrome）[2]ではVEPの必要性が高いと考えられる．ルーチンで行われるVEPは白黒の格子縞パターン（checkerboard pattern）刺激によるVEPであり，P100潜時の延長の有無を視神経障害（脱髄による視

Key words

P100

パターン刺激提示後100ミリ秒後に頂点を認める陽性波形．脳波上は慣習的に下向きの波形を陽性波，上向きの波形を陰性波としている．"P"はpositive（陽性）であることを表す．P100は一次視覚野由来の反応であると考えられている[5,6]．

1 VEP 所見と臨床症状との対応

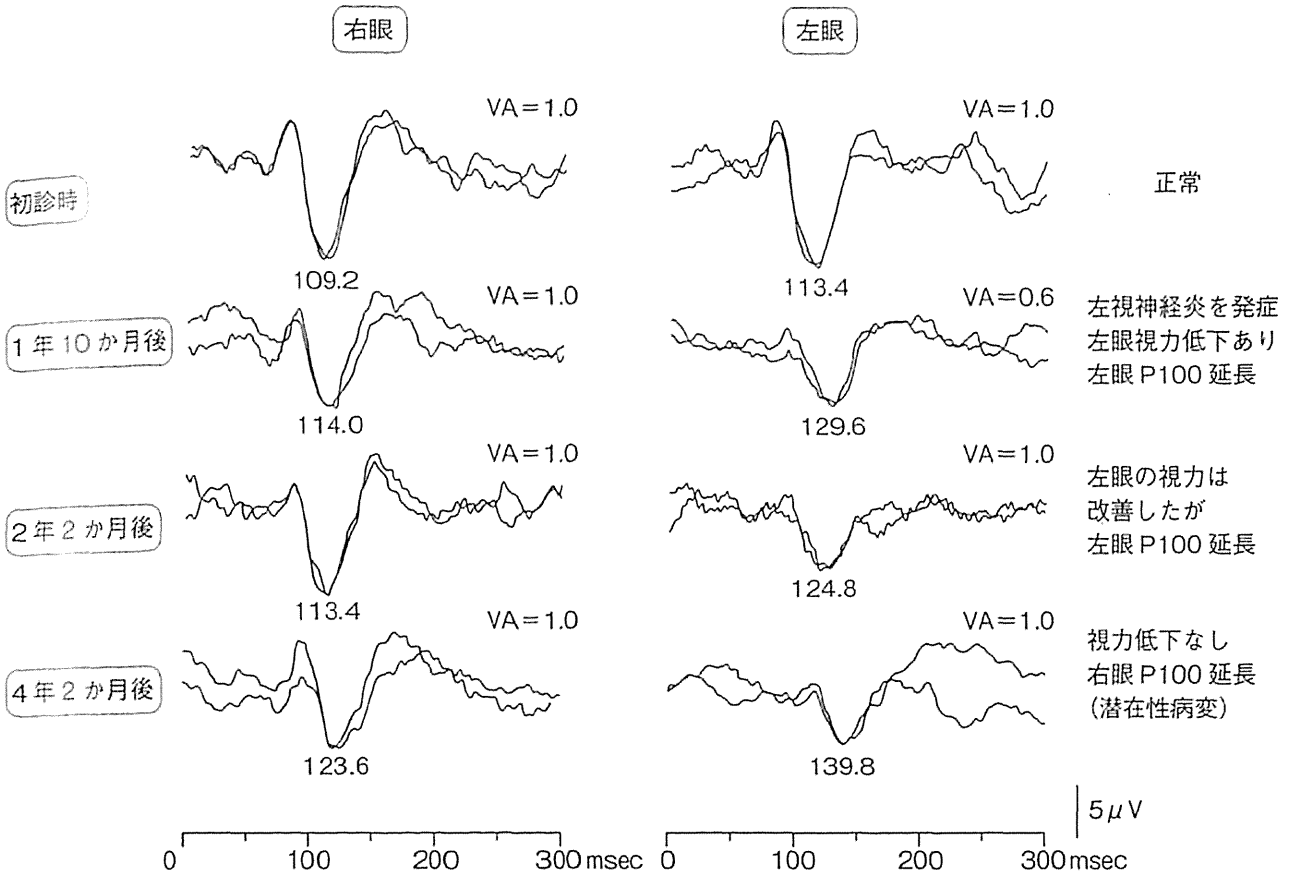

(飛松省三．臨床脳波 2005[3] を改変)

神経の伝導遅延）の判定の指標としている（**1**）．注意すべき点として，臨床的に視力が改善しても VEP 所見の変化は緩慢であり，治療効果の速やかな判定は難しいことが多い（**1**）．

体性感覚誘発電位（SEP）

SEP は体性感覚系の機能的な評価を行う検査であり，他の誘発電位検査と同様に，画像で検出し得ない病変の検出に有効である．SEP は，上肢（正中，尺骨神経）あるいは下肢（後脛骨，総腓骨神経）の末梢神経を皮膚表面から電気刺激して記録する．求心性感覚経路には後索–内側毛帯系と脊髄視床路系があり，前者は主に識別性の触覚・振動覚・関節位置覚を伝え，後者は痛覚・温度覚を伝えているが，電気刺激で行うルーチンの SEP で評価できるのは前者の経路であることに留意する必要がある．

正中神経を手根部で刺激すると，鎖骨上窩（Erb 点）に設置した電極から N9，頸椎棘突起上では N13，手の感覚野に対応する頭皮上では N20 が記録される．N9，N13，N20 の発生源はそれぞれ上腕神経叢，頸髄後角，大脳皮質感覚野（中心後回皮質 3b 野）とされている[8,9]．後脛骨神経刺激を足関節部で刺激すると，第 4 腰椎棘突起上から N17，第 12 胸椎棘突起上から N20，足の感覚野に対応する頭皮上から P37 が記録される（文献[8] によって，N20

Column

なぜパターン刺激か？

白黒の格子縞を1 Hz 程度で反転させて記録するパターンVEP が視神経炎の診断に有用であることが1972年に報告されて以来[4]，この方法が標準的な記録法となっている．パターン刺激以外の刺激方法として閃光（フラッシュ）刺激もあるが，一般に波形の再現性が悪い．網膜神経節細胞は同心円状の受容野をもち，受容野の中心部に光刺激が加わると興奮するが，受容野の周辺部に光刺激が加わると逆に抑制され，両者は拮抗関係にある（**2**）．格子の大きさがちょうど受容野の中心部だけに当たる大きさであれば反応が大きくなるが，格子が大きすぎると周辺部も刺激してしまうため，反応が抑制されて小さくなってしまう．反対に格子が小さすぎると中心部が十分に刺激されず，反応は小さくなる．すなわち，網膜神経節細胞を適切に刺激するには，刺激のコントラストや大きさが重要である[5,6]．

神経節細胞の受容野は網膜の黄斑部に近いほど小さく，細かい視覚情報を検出できる．黄斑部神経細胞の受容野の大きさは視角20分以下である．視角とは，視覚情報（刺激）の大きさと視距離から規定される，度や分で表現される尺度である（1分は1度の1/60）．当院では視角30分と15分の2つの格子サイズを用いている．また，ヒトの黄斑部を十分に刺激できる刺激視野の大きさは視角8度であり，刺激視野がその大きさになるよう設定する．なお，格子幅30分とは114 cm の視距離で一辺の長さが1 cm，視野8度とは16 cm にそれぞれ相当する．

2 網膜神経節細胞の受容野とパターン刺激の関係

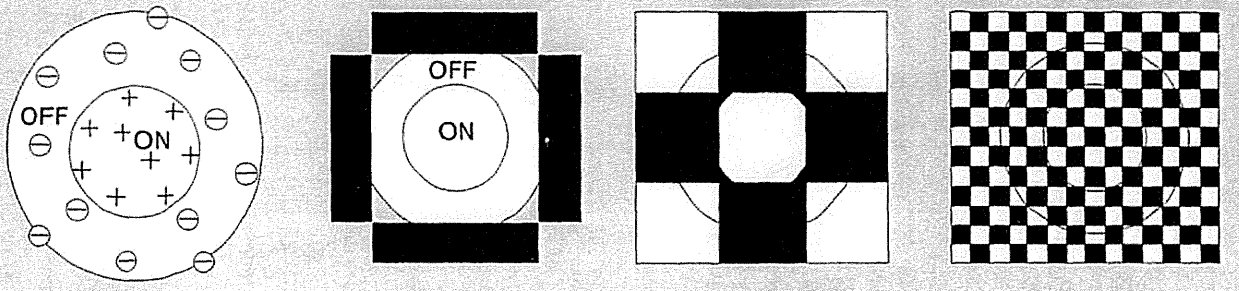

受容野　×格子が大きい（OFFにより反応抑制）　○適切な格子幅　×格子が小さい（ON刺激が不十分）

（飛松省三．臨床脳波 2005[3] を改変）

Column

抗アクアポリン4（AQP4）抗体とVEP所見の関係

抗AQP4 抗体陽性例の視神経脊髄型MS では視神経障害がより高度であることが知られているが，それを電気生理学的なアプローチから考察した報告がある．Watanabe ら[7] は抗AQP4 抗体陽性例と陰性例のVEP所見の違いを検討し，陰性例ではP100 潜時の延長例が多いのに対し，陽性例では誘発困難例が有意に多く認められることを報告した（**3**）．一般的に，潜時延長のみの場合は脱髄を中心とした障害が示唆され，誘発困難な場合は軸索障害が生じた場合ないしは高度の脱髄により反応ピークの時間的なばらつき（時間的分散という）が高度な場合が示唆される．抗AQP4 抗体が病態に関与している場合は組織の炎症と浮腫性変化が遷延しやすく，視神経管部での絞扼により虚血性の障害を受けやすいことが考えられ，その結果として誘発困難例が多いのではないかと推察される．

3 抗AQP4 抗体陽性例と陰性例におけるVEP所見の特徴

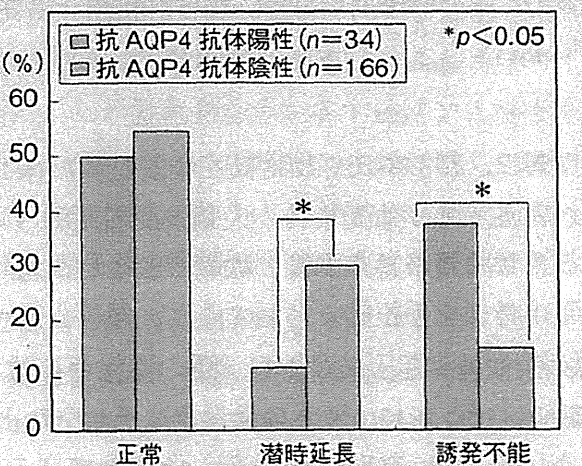

（Watanabe A, et al. *J Neurol Sci* 2009[7] より）

4 MS 患者における上肢 SEP 所見例

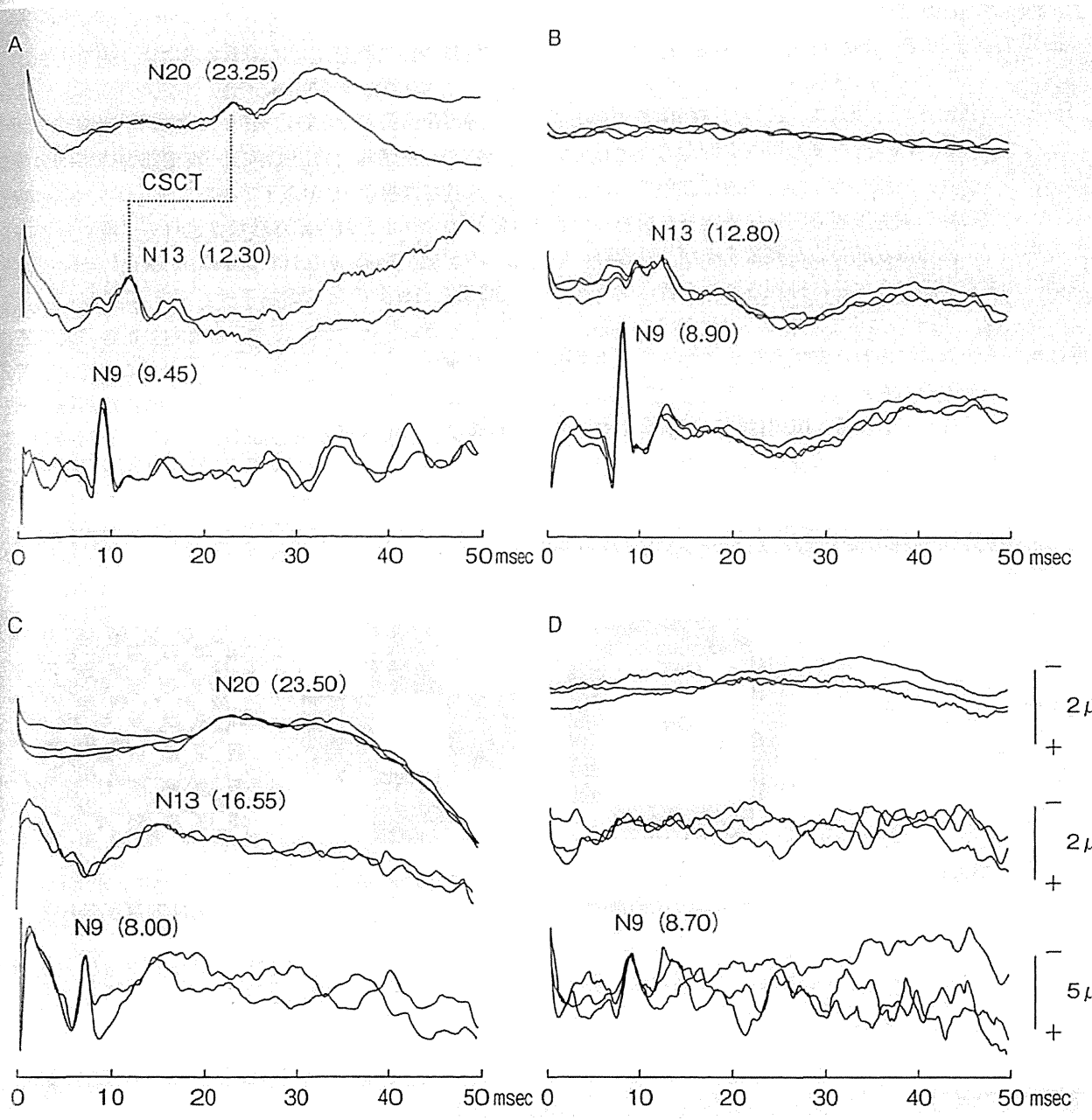

A：下部頸髄より上位の中枢病変．N20 潜時の延長（> 21.45 msec）および CSCT の延長（23.25 − 12.30 = 10.95 msec > 7.33 msec）を認める．B：下部頸髄より上位の中枢病変（高度）．N20 が誘発されない．C：下部頸髄病変．N13 および N20 が延長しているが，CSCT は正常．D：下部頸髄病変（高度）．N13 および N20 消失．

（萩原綱一ほか．多発性硬化症の診断と治療，2008[10] を改変）

は N22，P37 は P39 と記載されている）．N17，N20，P37 の発生源はそれぞれ馬尾，腰～仙髄後角，大脳皮質感覚野（中心後回皮質 3b 野）である[8,9]．各誘発成分の頂点潜時・振幅，および N20 と N13 の潜時差から中枢感覚伝導時間（central sensory conduction time：CSCT）を測定して感覚障害の高位診断を行うことができる（**4**）．MS で重要となるのは CSCT であるが，脊髄病変により N13 や下肢 SEP の N20 において異常を認めるパターンもある．

運動誘発電位（MEP）

磁気刺激を用いて運動神経遠心路の神経伝導時間を評価する検査法であ

Key words

中枢感覚伝導時間（CSCT）

上肢 SEP においては N20（体性感覚野の手領域）の潜時から N13（頸髄後角）の潜時を引き算した値を CSCT と定義している．下肢 SEP の場合は P37（体性感覚野の足領域）の潜時から N20（腰～仙髄後角）の潜時を引いた値が CSCT である．CSCT は身長や上下肢長の影響をほとんど受けない．

Column

なぜ電気刺激か？

触覚，痛覚，振動覚，温度覚といった感覚種別の機械的刺激を用いると，それぞれの感覚に対応した求心線維のインパルスを発生させることができる．神経学的診察による所見と対応づけるためには，こうした感覚種別の刺激を用いて検査できればそれに越したことはない．しかしながら，こうした感覚種別の刺激装置を用いた場合，刺激の立ち上がり（刺激開始から刺激が最大になるまでの時間）が遅く，かつ刺激される機械受容器の数が少ないため，得られる反応は低振幅になってしまう．一方で電気刺激を用いた場合は多種類の末梢神経線維を同時に刺激してしまうが，伝導速度が速い大径有髄線維を優先して興奮させることにより，得られる反応の振幅が大きく安定する．ただし，伝導速度が速い大径有髄線維の多くは識別性の触覚・振動覚・関節位置覚に関わる線維であり，そのためルーチンで行われている電気刺激によるSEPでは主に後索-内側毛帯系の機能を評価していることに留意する必要がある．

5 MS 患者における上肢 MEP 所見

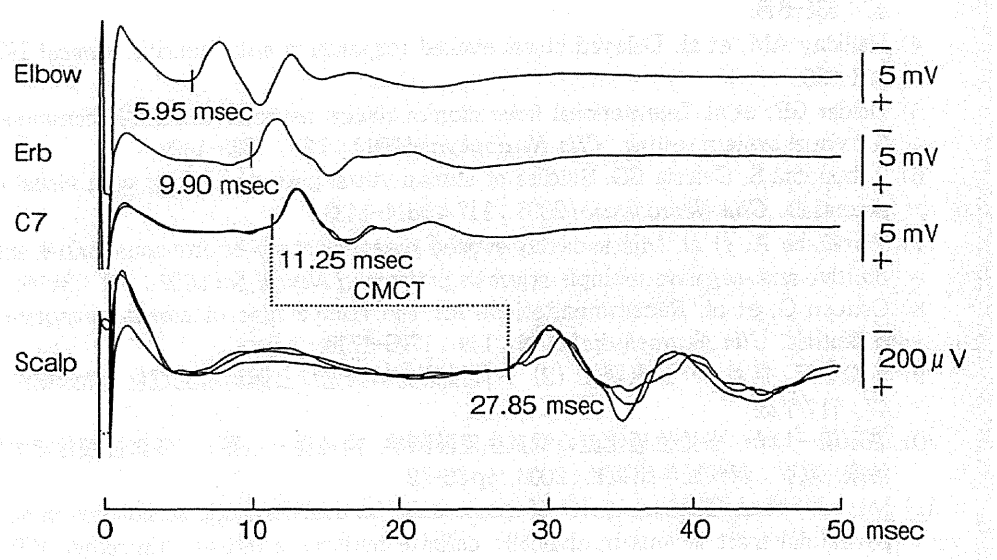

Elbow 刺激，Erb 点刺激，頸部（C7）刺激における各 MEP 潜時は正常であるが，CMCT が 27.85 − 11.25 ＝ 16.60 msec（＞ 10.67 msec）と延長しており，錐体路における伝導遅延が示唆される．

（萩原綱一ほか．多発性硬化症の診断と治療，2008[10] を改変）

Key words

中枢運動伝導時間（CMCT）

上肢 MEP では経頭蓋・運動野刺激 MEP と頸部（C7）刺激 MEP の立ち上がり潜時の差，下肢 MEP では経頭蓋・運動野刺激 MEP と腰部（L4）刺激 MEP の立ち上がり潜時の差が CMCT として算出される．頸部刺激での興奮部位は前角細胞ではなく椎間孔付近の神経根であると推定されているため，CMCT は純粋な錐体路伝導時間ではない．また，下肢 MEP についても腰部刺激 MEP は神経根を刺激しているため，同様のことがいえる．臨床上は CMCT を錐体路障害の指標として用いても差し支えないが，厳密には神経伝導検査における F 波潜時に異常がないことを確認する必要がある．

る．磁気刺激では電気刺激のような痛みを伴わず，頭皮・頭蓋骨・脳脊髄液などの電気抵抗の影響を受けずに大脳皮質運動野を興奮させることが可能である．上肢 MEP では肘部正中神経（Elbow），Erb 点，頸部（C7），手の運動野（Scalp）を順に刺激し，短母指外転筋から MEP を記録する．それぞれの刺激部位について MEP の立ち上がり潜時を計測し，運動機能障害の高位診断を行うことができる．特に頸部（C7）刺激と手の運動野（Scalp）刺激の MEP 潜時の差から求められる中枢運動伝導時間（central motor conduction time：CMCT）は錐体路障害の指標として MS では重要である（**5**）．下肢 MEP では腰部神経根（L4）と足の運動野を刺激して母趾外転筋において MEP 潜時を計測する．MEP は VEP や SEP と比較して感度（異常検出率）の高い検査であるとされている[11,12]．ただし，MEP や SEP の場合，患者背景（頸椎症や末梢神経障害の有無など）をふまえて結果を解釈しなければ特異性が失われてしまうことに注意が必要である．また，深部腱反射の亢進や

病的反射の出現とMEP所見の間には必ずしも相関がみられないことや，VEPやSEPと同様に治療に対する変化は緩慢であることに留意する必要がある．

（萩原綱一，飛松省三）

文献

1) Gronseth GS, Ashman EJ. Practice parameter: The usefulness of evoked potentials in identifying clinically silent lesions in patients with suspected multiple sclerosis (an evidence-based review) : Report of the Quality Standards Subcommittee of the American Academy of Neurology. *Neurology* 2000 ; 54 : 1720-1725.
2) Lebrun C, et al. Association between clinical conversion to multiple sclerosis in radiologically isolated syndrome and magnetic resonance imaging, cerebrospinal fluid, and visual evoked potential: Follow-up of 70 patients. *Arch Neurol* 2009 ; 66 : 841-846.
3) 飛松省三．早わかり誘発電位（2）—視覚誘発電位と聴覚脳幹誘発電位．臨床脳波 2005 ; 47 : 638-648.
4) Halliday AM, et al. Delayed visual evoked response in optic neuritis. *Lancet* 1972 ; 1 : 982-985.
5) Holder GE, et al. International federation of clinical neurophysiology: Recommendations for visual system testing. *Clin Neurophysiol* 2010 ; 121 : 1393-1409.
6) Tobimatsu S, Celesia GG. Studies of human visual pathophysiology with visual evoked potentials. *Clin Neurophysiol* 2006 ; 117 : 1414-1433.
7) Watanabe A, et al. Multimodality-evoked potential study of anti-aquaporin-4 antibody-positive and -negative multiple sclerosis patients. *J Neurol Sci* 2009 ; 281 : 34-40.
8) Cruccu G, et al. Recommendations for the clinical use of somatosensory-evoked potentials. *Clin Neurophysiol* 2008 ; 119 : 1705-1719.
9) 飛松省三．早わかり誘発電位（3）—体性感覚誘発電位と運動誘発電位．臨床脳波 2005 ; 47 : 717-726.
10) 萩原綱一ほか．多発性硬化症の電気生理診断学．吉良潤一（編），多発性硬化症の診断と治療．東京：新興医学出版社 ; 2008, pp.66-72.
11) Mayr N, et al. The sensitivity of transcranial cortical magnetic stimulation in detecting pyramidal tract lesions in clinically definite multiple sclerosis. *Neurology* 1991 ; 41 : 566-569.
12) 黒川智美ほか．電気生理学的診断法．日本臨牀 2003 ; 61 : 1347-1354.

Further reading

- 飛松省三．早わかり誘発電位（1）—誘発電位の基礎．臨床脳波 2005 ; 47 : 573-583.
  誘発電位に必要な生理学的知識，誘発電位の記録と解析法，トラブル対処法などを中心に解説．

Clinical Neurophysiology 125 (2014) 1021–1029

Contents lists available at ScienceDirect

Clinical Neurophysiology

journal homepage: www.elsevier.com/locate/clinph

Age-related changes across the primary and secondary somatosensory areas: An analysis of neuromagnetic oscillatory activities

Koichi Hagiwara [a,*], Katsuya Ogata [a], Tsuyoshi Okamoto [b], Taira Uehara [c], Naruhito Hironaga [a], Hiroshi Shigeto [c], Jun-ichi Kira [c], Shozo Tobimatsu [a]

[a] Department of Clinical Neurophysiology, Neurological Institute, Faculty of Medical Sciences, Kyushu University, Fukuoka, Japan
[b] Faculty of Medical Sciences, Kyushu University, Fukuoka, Japan
[c] Department of Neurology, Neurological Institute, Faculty of Medical Sciences, Kyushu University, Fukuoka, Japan

ARTICLE INFO

Article history:
Accepted 7 October 2013
Available online 1 November 2013

Keywords:
Secondary somatosensory area (SII)
Aging
Oscillatory activity
Phase-locking factor (PLF)
Weighted phase-lag index (wPLI)
Cortical disinhibition

HIGHLIGHTS

- We recorded somatosensory evoked magnetic fields with oscillatory activity indices to evaluate the effects of aging on the primary (SI) and secondary (SII) somatosensory areas.
- The oscillatory activities well depicted the age-related cortical disinhibition across SI and SII.
- Our data provide the first evidence for age-related changes in cortical synchrony in SII.

ABSTRACT

Objective: Age-related changes are well documented in the primary somatosensory cortex (SI). Based on previous somatosensory evoked potential studies, the amplitude of N20 typically increases with age probably due to cortical disinhibition. However, less is known about age-related change in the secondary somatosensory cortex (SII). The current study quantified age-related changes across SI and SII mainly based on oscillatory activity indices measured with magnetoencephalography.
Methods: We recorded somatosensory evoked magnetic fields (SEFs) to right median nerve stimulation in healthy young and old subjects and assessed major SEF components. Then, we evaluated the phase-locking factor (PLF) for local field synchrony on neural oscillations and the weighted phase-lag index (wPLI) for cortico-cortical synchrony between SI and SII.
Results: PLF was significantly increased in SI along with the increased amplitude of N20m in the old subjects. PLF was also increased in SII associated with a shortened peak latency of SEFs. wPLI analysis revealed the increased coherent activity between SI and SII.
Conclusions: Our results suggest that the functional coupling between SI and SII is influenced by the cortical disinhibition due to normal aging.
Significance: We provide the first electrophysiological evidence for age-related changes in oscillatory neural activities across the somatosensory areas.

1. Introduction

Age-related changes in the primary somatosensory area (SI) have been reported by a number of studies on somatosensory evoked potentials (SEPs). The most notable finding of SEPs in normal aging is the increased amplitude of the N20 component, which is the initial cortical response following electrical stimulation of the median nerve or fingers (Desmedt and Cheron, 1980, 1981; Drechsler, 1978; Tanosaki et al., 1999). The age-related electrophysiological changes in SI were also confirmed by magnetoencephalographic (MEG) studies, which demonstrated that the N20m component, an MEG counterpart of the N20 component (Wood et al., 1985), exhibited increased amplitude in the old (Huttunen et al., 1999; Stephen et al., 2006). Although the precise physiological mechanism has not been fully elucidated, the increased amplitude is probably caused by cortical disinhibition in the old (Drechsler, 1978; Huttunen et al., 1999; Stephen et al., 2006). In addition to the amplitude difference, the N20 latency is also prolonged in the old because of the slowing of conduction velocity in the peripheral nerves and spinal cord (Desmedt and

* Corresponding author. Address: Department of Clinical Neurophysiology, Neurological Institute, Faculty of Medical Sciences, Kyushu University, 3-1-1 Maidashi, Higashi-ku, Fukuoka 812-8582, Japan. Tel.: +81 92 642 5541; fax: +81 92 642 5545.
E-mail address: hagiwara-kyu@umin.ac.jp (K. Hagiwara).

1388-2457/$36.00
http://dx.doi.org/10.1016/j.clinph.2013.10.005

Cheron, 1980; Dorfman and Bosley, 1979). Thus, the age-related electrophysiological changes, up to the level of SI, have been well established.

Since somatosensory evoked magnetic fields (SEFs) can easily detect activity of the secondary somatosensory area (SII), many studies adopted SEFs to investigate the functional significance of SII. In contrast to SI, SII possesses higher cortical functions, such as sensorimotor integration, tactile discrimination, attention, perception of unified body image, and nociceptive information processing (for reviews, see Hari and Forss, 1999; Kakigi et al., 2000; Lin and Forss, 2002). In addition, it has been suggested that SII is unique in having dual afferent pathways. Several neurophysiological and anatomical studies have reported that SII receives input from SI as well as the thalamus (Karhu and Tesche, 1999; Lin and Forss, 2002; Raij et al., 2008; Zhang et al., 1996, 2001a, 2001b). A previous SEF study demonstrated an age-related reduction in source-wave amplitudes of SII using multi-dipole analysis (Stephen et al., 2006). However, a large number of averaging in their study was likely to have caused habituation, and the SII response did not appear for a relatively large number of subjects, which makes the results less conclusive. To our knowledge, there have been no ensuing studies conducted for assessing age-related changes in SII. Therefore, unlike the accumulating evidence on the age-related changes of SI, aging effects on SII have not been fully understood.

In the present study, we focused on oscillatory activities to evaluate the age-related changes across the somatosensory areas. We used two indices for synchronous neural oscillations: the phase-locking factor (PLF) and weighted phase-lag index (wPLI). PLF measures local phase synchrony with respect to incoming stimuli (Palva et al., 2005; Sinkkonen et al., 1995), whereas wPLI measures the consistency of the phase relationship between signals in separate areas while diminishing the effect of volume conduction (Vinck et al., 2011). A benefit of using these oscillatory activity indices is that both indices assess only the phase of the signals and are independent of amplitude (Sinkkonen et al., 1995; Vinck et al., 2011). We employed PLF as an index for local field synchrony in each somatosensory area (i.e., SI and SII), and wPLI as an index for functional connectivity between the two cortical areas. Here we consolidate the presence of aging effects on SII by utilizing those oscillatory activity indices in conjunction with the SEF analysis.

2. Methods

2.1. Subjects

Fifteen young volunteers (5 females; age, 29.0 ± 4.1 years; height, 171.0 ± 8.9 cm) and fifteen old volunteers (5 females; age, 63.7 ± 3.7 years; height, 162.0 ± 8.7 cm) participated in this study. All were right-handed and had no past medical history of neurological conditions. Prior to data collection, all participants gave written informed consent. This study was approved by the local ethics committee at Kyushu University.

2.2. Recording of neuromagnetic activity

The right median nerve was electrically stimulated at the wrist with constant current pulses of 0.2-ms duration. Intensity of the stimuli was adjusted above the motor threshold to produce slight contraction of the abductor pollicis brevis muscle. The interstimulus interval was pseudo-randomized (mean = 3 s). During the stimulation, continuous MEG signals were recorded using a whole-head 306-channel sensor array (Elekta, Neuromag) with 102 identical triple-sensor elements. Each triple-sensor element is composed of two orthogonally-oriented planar-type gradiometers and one magnetometer. Prior to recording, four head-position-indicator coils were attached to the subjects' head. Anatomical landmarks (nasion and bilateral preauricular points) and scalp shape were then digitized to construct a three-dimensional head coordinate system. At the beginning of the recording session, the subjects' head position was measured with respect to the center of the sensor array. The recording was performed while subjects lay in a supine position with their head positioned inside the helmet-shaped sensor array. During the recording, the subjects kept their eyes open, and their vigilance was monitored by MEG signals and a video camera positioned inside the shield room. Sampling rate was 5 kHz, with a 0.1–1500 Hz recording bandpass filter. A spatiotemporal signal space separation (tSSS) method (Taulu and Simola, 2006) was applied offline to the data to reduce external artifact signals. The data was downsampled to 1 kHz prior to the time–frequency analysis.

2.3. Data analysis

2.3.1. SEF analysis

SEFs were obtained by averaging approximately 100 responses offline. Trials exceeding 3000 fT/cm in amplitude were excluded before averaging. Root mean square (RMS) waveforms were reconstructed using each orthogonally-oriented pair of gradiometers (Hagiwara et al., 2010; Kida et al., 2006, 2007), and latencies and amplitudes were evaluated at sensors with maximal amplitude. Dipole moment was not assessed in this study because MRI was not obtained for all subjects. The waveforms were filtered at 0.3–150 Hz, and mean amplitude during the 50-ms pre-stimulus period was set as a baseline. We focused on the N20m component for the analysis of the SI response. With regard to SII, major components with bitemporal distribution peaking at around 70–120 ms (cSII for the contralateral response, and iSII for the ipsilateral one) were analyzed. The cSII response was reassured after subtracting the SI response using a signal space projection so that the waveform and isocontour map of cSII can be isolated (Hagiwara et al., 2010). Age-related differences for latencies were evaluated by an analysis of variance with age groups and height as covariate factors, and amplitudes were assessed by unpaired Student's *t*-test with respect to the age groups. In principle, this part of the analysis was conducted to determine sensors of interest for the following analysis of oscillatory activities in SI and SII.

2.3.2. Assessment of oscillatory activities within the somatosensory areas

Prior to this part of the analysis, we calculated vector sum signals from the raw data sets at each gradiometer pair, followed by continuous wavelet transformation for each single-trial data using complex Morlet to extract the time–frequency domain of the signals. The data at each time–frequency point was obtained at 1-Hz frequency resolution and 5-ms time resolution. We calculated two indices of neural synchrony: the phase-locking factor (PLF), which represents phase synchronization with respect to the stimuli, and the weighted phase-lag index (wPLI), which represents inter-areal phase synchrony.

To calculate PLF, we used the same computation method described by previous studies (Palva et al., 2005; Sinkkonen et al., 1995). Briefly, PLF was given by the following equation:

$$\mathrm{PLF} = \left| \frac{1}{N} \sum_{n=1}^{N} \frac{w_n(f,t)}{|w_n(f,t)|} \right|$$

where $w_n(f,t)$ represents the amplitude as well as the phase of a specific frequency f at a timepoint t, and N denotes the total epoch number. As seen in the equation, PLF yields only the phase of the signal whilst being unaffected by its amplitude. We used PLF as a measure to evaluate local field synchrony in SI and SII, which were represented by those at the sensors determined from the SEF analysis.

The second synchronization index, wPLI, was employed for the evaluation of inter-areal connectivity. The original idea of PLI was initially introduced by Stam et al. (2007) as a measure to isolate truly synchronous signals by using an imaginary component of the cross-spectrum. More precisely, it detects non-zero but consistent phase-differences between signals, as such zero phase-differences are considered to reflect common source or volume conduction-related false synchrony, which often contaminates other synchronization indices, such as coherence and phase-locking value. Subsequently, wPLI was proposed by Vinck et al. (2011) as an advanced method of PLI to improve specificity as well as robustness to noise and the volume conduction-related artifacts. A computation tool for the wPLI analysis has been provided by FieldTrip (fieldtrip.fcdonders.nl), an open-source MATLAB-based toolbox (Oostenveld et al., 2011). We employed the SI sensor as a reference for assessing wPLI between SI and bilateral SIIs, and the cSII sensor for wPLI between cSII and iSII. Note that wPLIs between the SI and cSII sensors were the same for both analyses, because directionality was not considered in this method. Baseline was corrected by subtracting the mean within the time window of −200 ms to −100 ms both in the PLF and wPLI analyses. For statistical comparison we first assessed the time–frequency region of interest (ROI) by conducting point-by-point *t*-tests for each value in the time–frequency resolution as mentioned above, and then sought out the meaningful ROI with contiguous activity. Statistical differences were considered significant at $p < 0.05$.

3. Results

3.1. SEFs of SI

The earliest peak in SI, the N20m component, was detected in all subjects (Figs. 1 and 2). Concerning the latency, there were main effects for the age group and height without any significant interaction effect. Thus, N20m showed prolonged latency in the old subjects (22.0 ± 1.0 vs. 23.1 ± 1.5 ms; $F(1, 26) = 11.8$, $p < 0.01$) even when the significant effect of height on latency ($F(1, 26) = 5.6$, $p < 0.05$) was taken into account. Amplitude analysis also showed a significant correlation with age (51.8 ± 18.9 vs. 96.6 ± 59.3 fT/cm; $p < 0.01$), with the old subjects showing larger responses than the young subjects. Although middle-latency components such as P35m and P60m were seen, these components were variable from subject to subject and were not significantly different between the two age groups.

3.2. SEFs of SII

Major components of SII were evoked bilaterally in the temporal regions, and peaked at around 70–120 ms (Figs. 1 and 2). Both cSII and iSII responses were identified in all subjects. The cSII responses exhibited significantly shortened latency in the old subjects (97.6 ± 17.6 vs. 81.3 ± 7.1 ms; $F(1, 26) = 5.6$, $p < 0.05$). The iSII responses also showed shorter latency in the old subjects compared with the young subjects (114.9 ± 24.6 vs. 93.9 ± 14.9 ms; $F(1, 26) = 4.3$, $p < 0.05$). As shown in Figs. 1 and 2, the old subjects exhibited steeper waveforms compared with the young subjects. Height was not a significant factor for the latency difference between the subject groups. Regarding the amplitude, there was no significant change with age.

3.3. PLFs of SI and SII

The PLF analysis revealed phase-locked activities in the SI and SII regions which corresponded to those in the SEF analysis (Fig. 3A). They were observed in a broad-frequency range from alpha to high gamma in both areas, with those in SII being

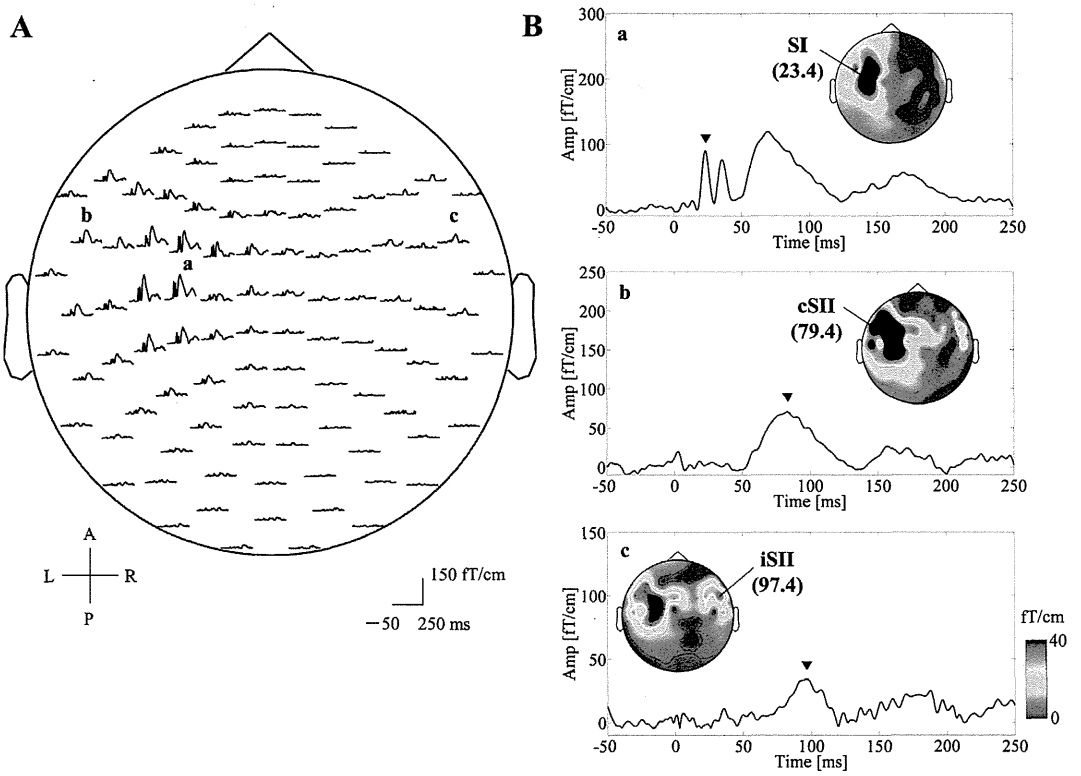

Fig. 1. SEFs in a representative young subject. (A) A plot of all sensors. Note that RMSs are computed for each pair of gradiometers. Small letters (i.e., a, b, c) represent the sensors showing maximal amplitudes for SI, cSII, and iSII, respectively. (B) Enlarged figures for the sensors marked with the small letters. Isocontour maps at the peak latencies are also displayed.